Article

SOURCE DATA | TRANSPARENT PROCESS

THE EMBO JOURNAL

Phosphoproteomics reveals a distinctive Mec1/ATR signaling response upon DNA end hyper-resection

Ethan J Sanford[1], William J Comstock[1], Vitor M Faça[1,2], Stephanie C Vega[1], Robert Gnügge[3], Lorraine S Symington[3] & Marcus B Smolka[1,*]

Abstract

The Mec1/ATR kinase is crucial for genome maintenance in response to a range of genotoxic insults, but it remains unclear how it promotes context-dependent signaling and DNA repair. Using phosphoproteomic analyses, we uncovered a distinctive Mec1/ATR signaling response triggered by extensive nucleolytic processing (resection) of DNA ends. Budding yeast cells lacking Rad9, a checkpoint adaptor and an inhibitor of resection, exhibit a selective increase in Mec1-dependent phosphorylation of proteins associated with single-strand DNA (ssDNA) transactions, including the ssDNA-binding protein Rfa2, the translocase/ubiquitin ligase Uls1, and the Sgs1-Top3-Rmi1 (STR) complex that regulates homologous recombination (HR). Extensive Mec1-dependent phosphorylation of the STR complex, mostly on the Sgs1 helicase subunit, promotes an interaction between STR and the DNA repair scaffolding protein Dpb11. Fusion of Sgs1 to phosphopeptide-binding domains of Dpb11 strongly impairs HR-mediated repair, supporting a model whereby Mec1 signaling regulates STR upon hyper-resection to influence recombination outcomes. Overall, the identification of a distinct Mec1 signaling response triggered by hyper-resection highlights the multi-faceted action of this kinase in the coordination of checkpoint signaling and HR-mediated DNA repair.

Keywords Dpb11; homologous recombination; Mec1; resection; Sgs1
Subject Categories DNA Replication, Recombination & Repair; Post-translational Modifications & Proteolysis; Proteomics
DOI 10.15252/embj.2020104566 | Received 27 January 2020 | Revised 16 February 2021 | Accepted 22 February 2021 | Published online 25 March 2021
The EMBO Journal (2021) 40: e104566

Introduction

In eukaryotes, PI3K-like kinases (PIKKs) play essential roles in the sensing of DNA damage and the coordination of cell cycle checkpoint activation and DNA repair mechanisms to maintain genome stability (Savitsky *et al,* 1995; Shiloh, 2003). In *Saccharomyces cerevisiae*, the Mec1 PIKK (human ATR) plays a central role in coordinating the response to DNA lesions that result in single-stranded DNA (ssDNA) exposure, including stalled replication forks and recessed double-strand breaks (DSBs) (Cha & Kleckner, 2002; Tercero *et al,* 2003; Segurado & Diffley, 2008; Deshpande *et al,* 2017). Mec1 senses ssDNA exposure through the recognition of replication protein A (RPA)-bound ssDNA via its obligate cofactor Ddc2 (human ATRIP) (Paciotti *et al,* 2000; Zou & Elledge, 2003; Deshpande *et al,* 2017). Once recruited to ssDNA, the activation of Mec1 requires the action of Mec1-activating proteins that contain Mec1 activation domains (MADs). Three Mec1 activators have been identified in budding yeast to date: Ddc1, a member of the 9-1-1 PCNA-like clamp; Dna2, a flap endonuclease with established roles in DNA end resection; and Dpb11, a multi-BRCT domain-containing scaffolding protein (Majka *et al,* 2006b; Mordes *et al,* 2008; Navadgi-Patil & Burgers, 2009; Kumar & Burgers, 2013; Wanrooij & Burgers, 2015). The substrate specificity of the activators is distinct—Dna2 recognizes DNA flaps, whereas Ddc1-Dpb11 is loaded onto 5′ dsDNA-ssDNA junctions produced directly, but not exclusively, as a result of DNA end resection (Majka *et al,* 2006a; Stewart *et al,* 2009).

Mec1 activates the downstream kinase Rad53 to mediate a DNA damage checkpoint response that arrests the cell cycle and reshapes the transcriptional and replication programs (Desany *et al,* 1998; Huang *et al,* 1998; Seeber *et al,* 2013; Lanz *et al,* 2019). Mec1 also phosphorylates a range of other targets to mediate checkpoint-independent responses (BastosdeOliveira *et al,* 2015; Lanz *et al,* 2018). Cells lacking Mec1, but not cells lacking Rad53, have high rates of gross chromosomal rearrangements (Myung *et al,* 2001), pointing to a crucial checkpoint-independent role for Mec1 in genome maintenance. Despite the importance of Mec1 for genome integrity, the mechanisms by which it suppresses genomic instabilities remain incompletely understood.

Recent biochemical and genetic evidence points to key roles for Mec1/ATR in the control of homologous recombination (HR) (Barlow & Rothstein, 2009; W.-L. Toh *et al,* 2010; Flott *et al,* 2011; Ullal *et al,* 2011; Dion *et al,* 2012; Liu *et al,* 2017), a multi-step DNA repair process essential for maintaining genome integrity during the S and G2 phases of the cell cycle (Moynahan & Jasin, 2010). The essential first step of HR is resection, the 5′–3′ nucleolytic degradation of DNA ends. Resection is followed by strand invasion, DNA synthesis, end

1 Department of Molecular Biology and Genetics, Weill Institute for Cell and Molecular Biology, Cornell University, Ithaca, NY, USA
2 Department of Biochemistry and Immunology and Cell-Based Therapy Center, Ribeirao Preto Medical School, University of Sao Paulo, Ribeirao Preto, Brazil
3 Department of Microbiology and Immunology, Columbia University Irving Medical Center, New York, NY, USA
*Corresponding author. Tel: +1 607 2550274; E-mail: mbs266@cornell.edu

ligation, and the processing of recombination intermediates such as Holliday junctions (Mimitou & Symington, 2009; West *et al,* 2016). Given its complexity, HR requires exquisite regulation to prevent deleterious outcomes. For example, strand invasion can occur at the wrong locus, leading to non-reciprocal translocations or other complex chromosomal rearrangements (Putnam & Kolodner, 2017).

Mec1 has been reported to control distinct steps in HR. Most notably, Mec1 plays both inhibitory and activating roles in the control of DNA end resection. Mec1 phosphorylation of histone H2A (γH2AX in mammals) and of the Ddc1 subunit of the 9-1-1 complex assembles a ternary complex involving the resection antagonist Rad9 at DNA lesions (Fig 1A). Mec1-dependent stabilization of Rad9 at DNA lesions antagonizes resection (Clerici *et al,* 2014; Liu *et al,* 2017). Mec1 also phosphorylates the DNA repair scaffold Slx4, which counteracts Rad9 recruitment and alleviates the block in resection (Ohouo *et al,* 2013; Dibitetto *et al,* 2015; Liu *et al,* 2017; Lanz *et al,* 2019). Therefore, Mec1 balances anti- and pro-resection factors for proper resection control. In addition, Mec1 phosphorylates the recombinase protein Rad51 to control HR through inactivation of Rad51 ATP hydrolysis and DNA-binding activities (Flott *et al,* 2011). It remains unknown whether Mec1 controls additional steps or proteins for HR control.

Dpb11, in addition to its role as an activator of Mec1 signaling, also functions as a key scaffolding protein to mediate the formation of ternary complexes involved in the DNA damage response. Dpb11 contains four BRCA1 C-terminus-like (BRCT) domains that act, often pairwise, to bind phosphorylated amino acid residues on client proteins (Wardlaw *et al,* 2014; Cussiol *et al,* 2015). To date, a number of Dpb11-interacting partners with roles in the DNA damage response have been identified, including the checkpoint mediator Rad9, the DNA repair scaffold Slx4, the nuclease Mus81-Mms4, and the chromatin remodeling protein Fun30 (Ohouo *et al,* 2010; Pfander & Diffley, 2011; Gritenaite *et al,* 2014; Bantele *et al,* 2017). By activating Mec1 and assembling these complexes, Dpb11 dictates the spatiotemporal dynamics of Mec1 signaling and its outcomes. Early in the response, Dpb11 bound to the checkpoint adaptor protein Rad9 mediates the transduction of signaling from Mec1 to the downstream checkpoint kinase Rad53, thereby establishing a cell cycle checkpoint response (Fig 1A; Schwartz *et al,* 2002; Pfander & Diffley, 2011). Dpb11-mediated stabilization of Rad9 at 5′ recessed ends of DNA lesions is also important to promote Rad9's function in blocking DNA end resection (Lazzaro *et al,* 2008; Liu *et al,* 2017; Villa *et al,* 2018). In the absence of Rad9, cells fail to properly activate the DNA damage checkpoint and DNA ends undergo rapid end resection (Lazzaro *et al,* 2008). Cells lacking Rad9 exhibit a greater incidence of non-allelic recombination, and this defect is consistent with the fact that loss of Rad9 frequently produces synergistic increases in chromosomal rearrangement in mutants lacking factors responsible for the regulation of homology-directed repair (Fasullo *et al,* 1998; Nielsen *et al,* 2013).

To explore additional roles for Mec1 in HR control, we monitored DNA damage signaling in cells lacking Rad9, which lack proper checkpoint signaling and DNA end protection, and therefore undergo extensive DNA end resection. Using phosphoproteomics, we find that *rad9*Δ cells exposed to DNA damage exhibit a specialized Mec1 signaling response converging toward the phosphorylation of proteins involved in ssDNA-associated transactions, including the ssDNA-binding heterotrimer RPA, the Sgs1 helicase, and the Uls1 translocase. In *rad9*Δ cells, Mec1 mediates an interaction between the STR (Sgs1-Top3-Rmi1) complex and the Dpb11 scaffold. We propose that, upon hyper-resection, Mec1 signaling regulates STR to influence recombination outcomes. Overall, the identification of a distinct Mec1 signaling response triggered by hyper-resection highlights the multi-faceted action of this kinase in the coordination of checkpoint signaling and HR-mediated DNA repair.

Results

Loss of Rad9 stimulates a specialized mode of Mec1 signaling

To explore checkpoint-independent roles of Mec1 downstream of resection control, we monitored Mec1-dependent signaling events in wild-type and *rad9*Δ cells treated with the DNA alkylating agent methylmethanesulfonate (MMS) or the radiomimetic drug phleomycin. Rad9 is known to play a key role in activating the downstream kinase Rad53 upon formation of ssDNA gaps by MMS or DSBs by phleomycin treatment (Fig 1A and B). Quantitative phosphoproteomics confirmed that Rad53 phosphorylation and Rad53-dependent phosphorylation events are impaired in *rad9*Δ cells (Fig 1C and Dataset EV1). Strikingly, the results show a set of phosphorylation events induced in *rad9*Δ cells, mostly on the preferential SQ/TQ motif for Mec1 or Tel1 phosphorylation (Fig 1C and D, and Dataset EV1). Analysis comparing *rad9*Δ cells with or without Mec1 confirmed that most of the SQ/TQ phosphorylation stimulated in *rad9*Δ cells is indeed dependent on Mec1 (Fig 1E and Dataset

Figure 1. A distinctive Mec1/ATR signaling response in *rad9*Δ cells.

A Model showing the role of Rad9 in activating the Rad53-dependent checkpoint and blocking DNA end resection. For simplicity, the ssDNA-binding heterotrimer RPA and the obligatory Mec1 cofactor Ddc2 have been omitted from the diagram.

B *rad9*Δ cells fail to activate the Rad53-dependent cell cycle checkpoint in the presence of either the DNA alkylating drug MMS (0.02%) or the radiomimetic drug phleomycin (40 μg/ml).

C Quantitative phosphoproteomic dataset showing phosphorylation sites enriched in cells lacking Rad9. Among the most highly enriched sites are Sgs1 T1269, Uls1 T540, Mec1 S1964, and 2 S-N sites in Rfa2. This response is similar in both the presence of 40 μg/ml phleomycin (*x*-axis) and 0.02% MMS (*y*-axis). Note downregulation of Rad53 signaling (red dots) due to the absence of Rad9.

D Pie chart showing that S/T-Q phosphorylation comprises a large fraction of *rad9*Δ-induced phosphorylation (71%), though only accounting for a small fraction (5%) of the entire dataset.

E Quantitative phosphoproteomic dataset showing that most phosphorylation events induced in *rad9*Δ cells are dependent on Mec1. These phosphoproteomic analyses were conducted in the presence of 0.02% MMS for 2 h.

F Model depicting Mec1-dependent phosphorylation of Sgs1, Uls1, and Rfa2 in response to hyper-resection in *rad9*Δ cells.

Source data are available online for this figure.

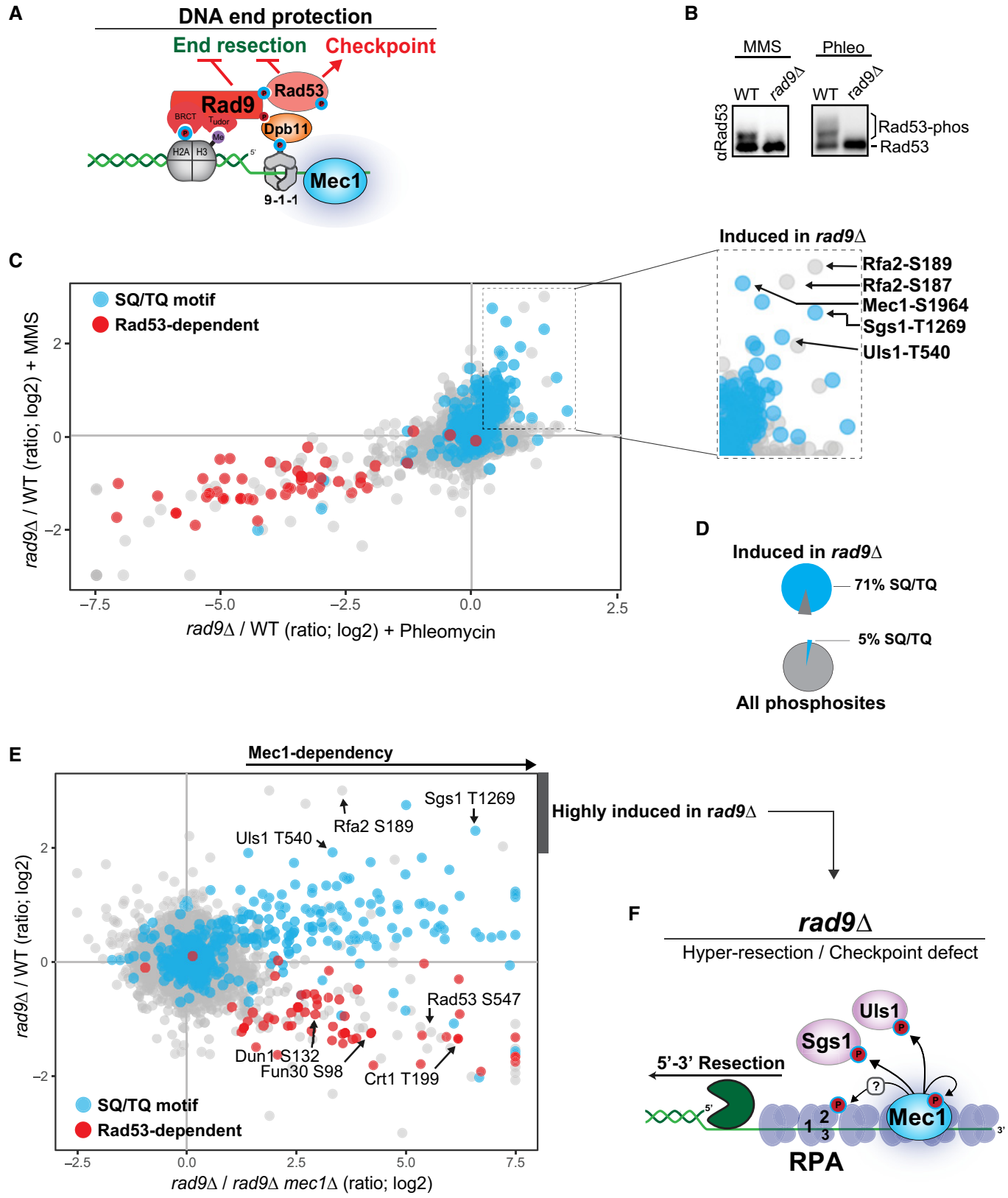
A
DNA end protection
End resection
Checkpoint
Rad9
Rad53
Dpb11
Mec1
9-1-1
BRCT
Tudor
H2A
H3
B
MMS
Phleo
WT
rad9Δ
αRad53
Rad53-phos
Rad53
C
SQ/TQ motif
Rad53-dependent
rad9Δ / WT (ratio; log2) + MMS
rad9Δ / WT (ratio; log2) + Phleomycin
Induced in rad9Δ
Rfa2-S189
Rfa2-S187
Mec1-S1964
Sgs1-T1269
Uls1-T540
D
Induced in rad9Δ
71% SQ/TQ
5% SQ/TQ
All phosphosites
E
Mec1-dependency
Highly induced in rad9Δ
Sgs1 T1269
Rfa2 S189
Uls1 T540
Rad53 S547
Dun1 S132
Fun30 S98
Crt1 T199
SQ/TQ motif
Rad53-dependent
rad9Δ / WT (ratio; log2)
rad9Δ / rad9Δ mec1Δ (ratio; log2)
F
rad9Δ
Hyper-resection / Checkpoint defect
Uls1
Sgs1
5'-3' Resection
Mec1
RPA

Figure 1.

EV1). Lack of Rad9 stimulated Mec1 autophosphorylation at S1964, but not autophosphorylation at S38, suggesting that in *rad9*Δ cells Mec1 adopts a distinct mode of activation/signaling compared with its mode of signaling in wild-type cells. The proteins with the strongest increases in Mec1-dependent phosphorylation in *rad9*Δ cells have been implicated in ssDNA-associated DNA repair transactions, including the ssDNA-binding protein Rfa2, the Sgs1 helicase, and the Uls1 translocase/ubiquitin ligase (Fig 1C, E and F, and Dataset EV1). Phosphorylation on Rfa2 was not on the SQ/TQ consensus, but on S-N and S-A sites, raising the possibility that Mec1 is either able to phosphorylate these other consensus motifs in the context of *rad9*Δ or that such sites are phosphorylated indirectly through the control of another kinase. Overall, our unbiased quantitative phosphoproteomic analyses reveal that the lack of the Rad9-induced resection block triggers a specialized Mec1 signaling response targeting proteins associated with HR-mediated DNA repair.

Contribution of the 9-1-1 complex and Dna2 for Mec1 activation in *rad9*Δ cells

Mec1 can be activated by two independent pathways—either by the 9-1-1 complex (formed by Ddc1-Rad17-Mec3 in *S. cerevisiae*) in conjunction with the Dpb11 scaffold, or by Dna2 (Mordes *et al,* 2008; Navadgi-Patil & Burgers, 2009; Kumar & Burgers, 2013; Wanrooij & Burgers, 2015). We sought to determine the contribution of each of these modes of Mec1 activation to the Mec1 signaling response stimulated in *rad9*Δ cells. We used quantitative mass spectrometry (MS) to determine the effect of deleting *DDC1,* which impairs 9-1-1/Dpb11-mediated Mec1 activation, or introducing the $DNA2^{WYAA}$ mutation, which fails to activate Dna2-dependent Mec1 signaling via mutations of residues W128 and Y130 in the Dna2 Mec1 activating domain (MAD) (Kumar & Burgers, 2013). Both mutants were analyzed in cells also lacking *RAD9*. Whereas the $DNA2^{WYAA}$ mutation had minimal effect on most Mec1-dependent phosphorylation (Fig 2B and C, and Dataset EV2), the deletion of *DDC1* resulted in stronger impairment of most Mec1-dependent signaling induced by MMS in *rad9*Δ cells (Fig 2A). Similarly, phosphorylation of Sgs1 by Mec1 was not altered by the $DNA2^{WYAA}$ mutation but was reduced by lack of Ddc1 (Fig 2C and Dataset EV2). The reduction in detected Sgs1 phosphorylation sites was not drastic, suggesting that Dna2-mediated Mec1 activation or another mode of Mec1 signaling may partially compensate for loss of Ddc1. Still, the reduction in *ddc1*Δ cells was comparable in magnitude to the increase in Sgs1 phosphorylation observed in *rad9*Δ cells, suggesting that the stimulation of the phosphorylation observed in *rad9*Δ cells is principally induced upon DNA damage via the 9-1-1-dependent pathway of Mec1 activation. We note, however, that the reduction in Sgs1 phosphorylation in *ddc1*Δ cells may be caused not only by impaired Mec1 activation, but also by impaired recruitment of Sgs1 to DNA lesions. Moreover, the $DNA2^{WYAA}$ mutation did result in some appreciable reduction, albeit minor, in Rfa2 S189 phosphorylation, suggesting some coordination between 9-1-1 and Dna2 in mediating distinct Mec1-dependent signaling events in *rad9*Δ cells.

Ablation of resection factors Dna2 and Exo1 impairs Mec1 phosphorylation of ssDNA-related proteins in *rad9*Δ cells

Since Rad9 is important to protect DNA ends by preventing resection (Lazzaro *et al,* 2008), a possible explanation for the increase in the phosphorylation of proteins involved in ssDNA-associated repair transactions in *rad9*Δ cells is that hyper-resection stimulates a distinct mode of Mec1 signaling. To test this model, we performed quantitative phosphoproteomics comparing *rad9*Δ cells to cells lacking both Rad9 and the long-range resection factors Dna2 and Exo1. Of note, we chose to ablate Dna2, and not Sgs1, because Sgs1 is one of the Mec1 targets of interest. Since *DNA2* is an essential gene, we used cells bearing an auxin-inducible degron (AID) allele of *DNA2* (Fig EV1A and B; Nishimura *et al,* 2009). The experimental scheme for phosphoproteomic analysis of long-range resection dependency of the *rad9*Δ-dependent Mec1 signaling response is outlined in Fig EV1C. Since these cells are prototrophic for arginine, we were unable to use the same SILAC-based quantitation we used in all other phosphoproteomic analyses, and opted instead to use TMT-based quantitation (Han *et al,* 2001; Dayon *et al,* 2008; Zhang & Elias, 2017). As shown in Fig 2D (and Fig EV1D, and Datasets EV2 and EV3), the ablation of Exo1 and Dna2 function resulted in consistent reduction in the phosphorylation of several Mec1-dependent S/T-Q phosphorylation events, with some of the more striking reductions occurring at the sites in Sgs1, Uls1, and Rfa2 found to be up-regulated in *rad9*Δ cells. Given the known issues of ratio compression associated with TMT-based quantitation (Hogrebe *et al,* 2018), especially when using MS2 for quantitation as in our case, the fold changes are noticeably reduced relative to SILAC-based quantitation. Our data are therefore likely underestimating the true dependency of these events on long-range resection. These results are consistent with the model that, upon loss of Rad9, hyper-resection causes a distinct mode of Mec1 signaling that includes increased phosphorylation of factors associated with ssDNA transactions, including Sgs1, Uls1, and Rfa2 (Fig 1F).

The STR complex undergoes extensive Mec1-dependent phosphorylation in *rad9*Δ cells

Sgs1 is a well-established regulator of homology-directed repair (Chiolo *et al,* 2005; Lo *et al,* 2006; Ashton *et al,* 2011; Mirzaei *et al,* 2011; Klein & Symington, 2012; Bermúdez-López *et al,* 2016; Campos-Doerfler *et al,* 2018). Given the key roles for Sgs1 in multiple steps of HR control, including resection, heteroduplex rejection, and joint molecule dissolution, we decided to further investigate Mec1-dependent phosphorylation of Sgs1. Data from a recently deposited phosphoproteome database reveal that Sgs1 is phosphorylated at multiple sites (Fig 3A; Lanz *et al,* 2021). In addition to the sites detected in our phosphoproteomic experiments (Fig 1), we noticed that most of the other previously identified phosphorylation sites in Sgs1 cluster at the N-terminus, which contains a large unstructured region previously reported to engage in a range of protein–protein interactions (Bjergbaek *et al,* 2005; Chiolo *et al,* 2005; Hegnauer *et al,* 2012). Analysis of a previously reported, stable, Sgs1 truncation spanning the first 647 amino acids ($Sgs1^{1–647}$; Mirzaei *et al,* 2011) revealed that upon MMS treatment, the Sgs1 N-terminus undergoes a stronger MMS-induced gel mobility shift in *rad9*Δ cells than in wild-type cells (Fig 3B, left). Consistent with the finding that Sgs1 undergoes Mec1-dependent hyper-phosphorylation in *rad9*Δ cells (Fig 1), the gel mobility shift of the $Sgs1^{1–647}$ truncation in *rad9*Δ cells was severely reduced in cells lacking Mec1 (Fig 3B, right). These results confirm that Sgs1 becomes preferentially phosphorylated in a Mec1-dependent

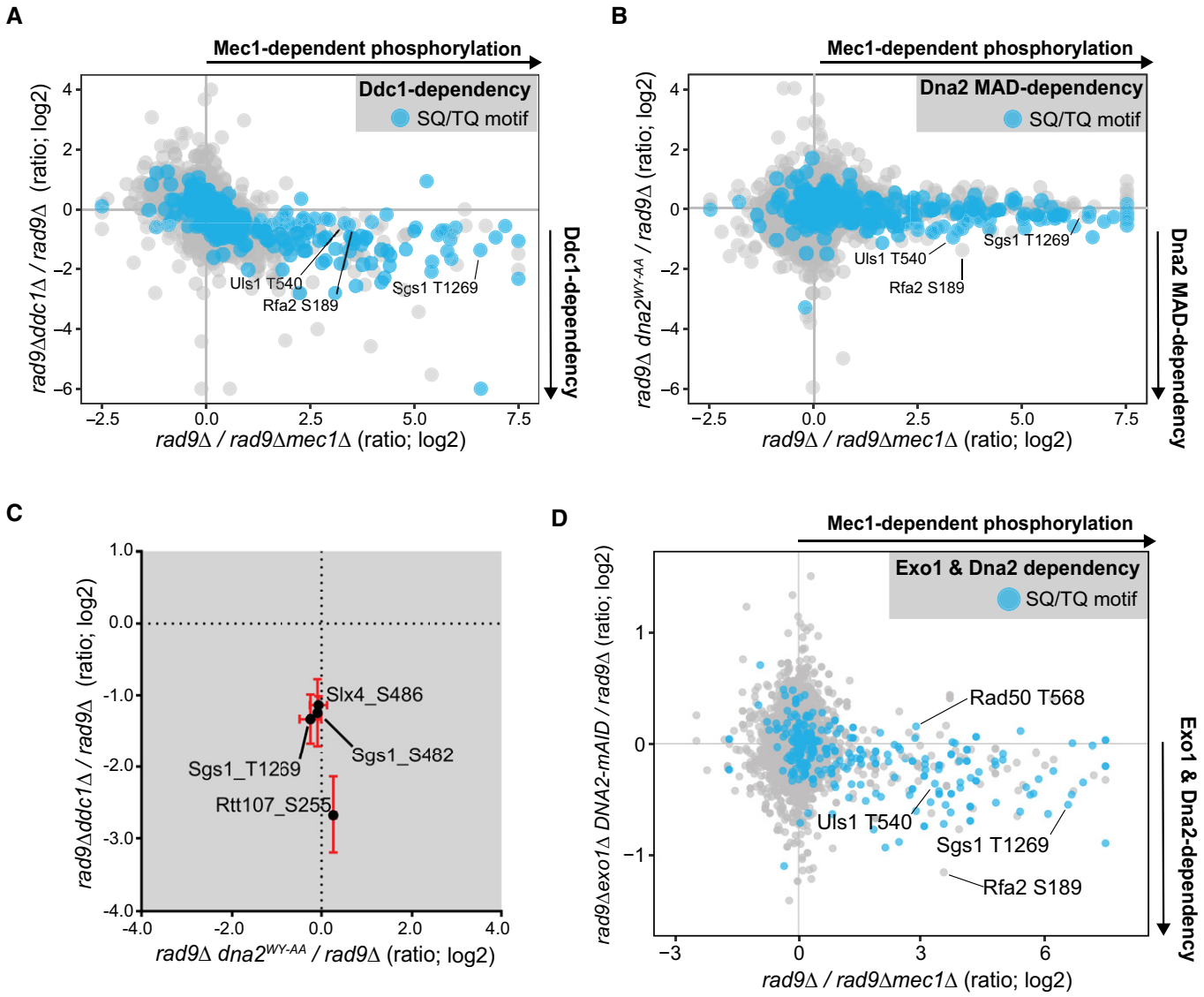

Figure 2. The 9-1-1 subunit Ddc1 plays a more prominent role in activation of Mec1 in response to *rad9*Δ than Dna2.

A Quantitative phosphoproteomic analysis defining the role of Ddc1 in Mec1-dependent phosphorylation in *rad9*Δ cells. Ddc1 dependency (*y*-axis) is plotted against Mec1 dependency (*x*-axis). These phosphoproteomic analyses were conducted in the presence of 0.02% MMS for 2 h.

B Quantitative phosphoproteomic analysis defining the role of Dna2 (WY-AA mutation impairs Mec1-activating function of Dna2) in the set of Mec1-dependent phosphorylation in *rad9*Δ cells. Dna2 Mec1 activation domain (MAD) dependency (*y*-axis) is plotted against Mec1 dependency (*x*-axis). These phosphoproteomic analyses were conducted in the presence of 0.02% MMS for 2 h.

C Plot comparing Dna2 and Ddc1 dependency of selected Mec1 substrates. Error bars represent standard deviation of two or more independent peptide-spectrum matches (PSMs) of the indicated site.

D Quantitative phosphoproteomic analysis defining the role of long-range resection factors Exo1 and Dna2 in Mec1-dependent phosphorylation events in *rad9*Δ cells. Mec1 dependency (x-axis) is plotted against long-range resection dependency (y-axis). These phosphoproteomic analyses were conducted in the presence of 0.02% MMS for 2 h. For the *DNA2-AID* cell line, cells were pretreated for 15 min with 100 μM IAA and then treated for 2 h with 0.02% MMS.

manner in cells lacking Rad9 and reveal that in addition to phosphorylation of threonine 1,269 identified in our phosphoproteomic analysis, the N-terminus of Sgs1 also undergoes extensive Mec1-dependent phosphorylation.

Next, we performed quantitative MS analysis of the N-terminal region of Sgs1 (residues 1–647) in order to map *rad9*Δ-dependent phosphorylation. Our analysis revealed that, while not all detected S/T-Q phosphorylation events were induced in cells lacking Rad9, threonine 585 phosphorylation (a TQ motif) was induced in the absence of Rad9 (Fig 3C and Dataset EV2). In addition, multiple phosphorylation sites of the S-N motif within a 100 amino acid window on the N-terminus of Sgs1 were highly induced in *rad9*Δ cells (Fig 3C and Dataset EV2), as well as phosphorylation on residues 348/358, 528, and 617, which are not in S/T-Q or S/T-N motifs. Our analyses indicate that the pattern of Sgs1 phosphorylation induced in *rad9*Δ cells is complex and includes non-S/T-Q

motifs. Moreover Rmi1 contains four S/T-Q motifs at S8, T77, T112, and T195. To determine whether Rmi1 was hyperphosphorylated in *rad9*Δ cells in the same manner as Sgs1, we analyzed by co-immunoprecipitation (Co-IP) the fraction of Rmi1 bound to Sgs1 (Fig 3D). While Rmi1 detectability was obscured in the input fraction due to a contaminating band at approximately the same molecular weight as the tagged protein, Rmi1 appears as a doublet when immunoprecipitated with Sgs1. We interpret the lower molecular weight band to be non(or hypo)-phosphorylated Rmi1, and the higher molecular weight band to be a phosphorylated species of Rmi1. Interestingly, the stoichiometry of Rmi1 phosphorylation changes in response to *rad9*Δ such that the intensity of the lower molecular weight band is reduced, indicating an increase in the phosphorylated species of the protein. Mutation of the four S/T-Q motifs to alanine (AQ mutant) abolishes the gel shift, consistent with these sites being targeted by Mec1. Overall, these results reveal

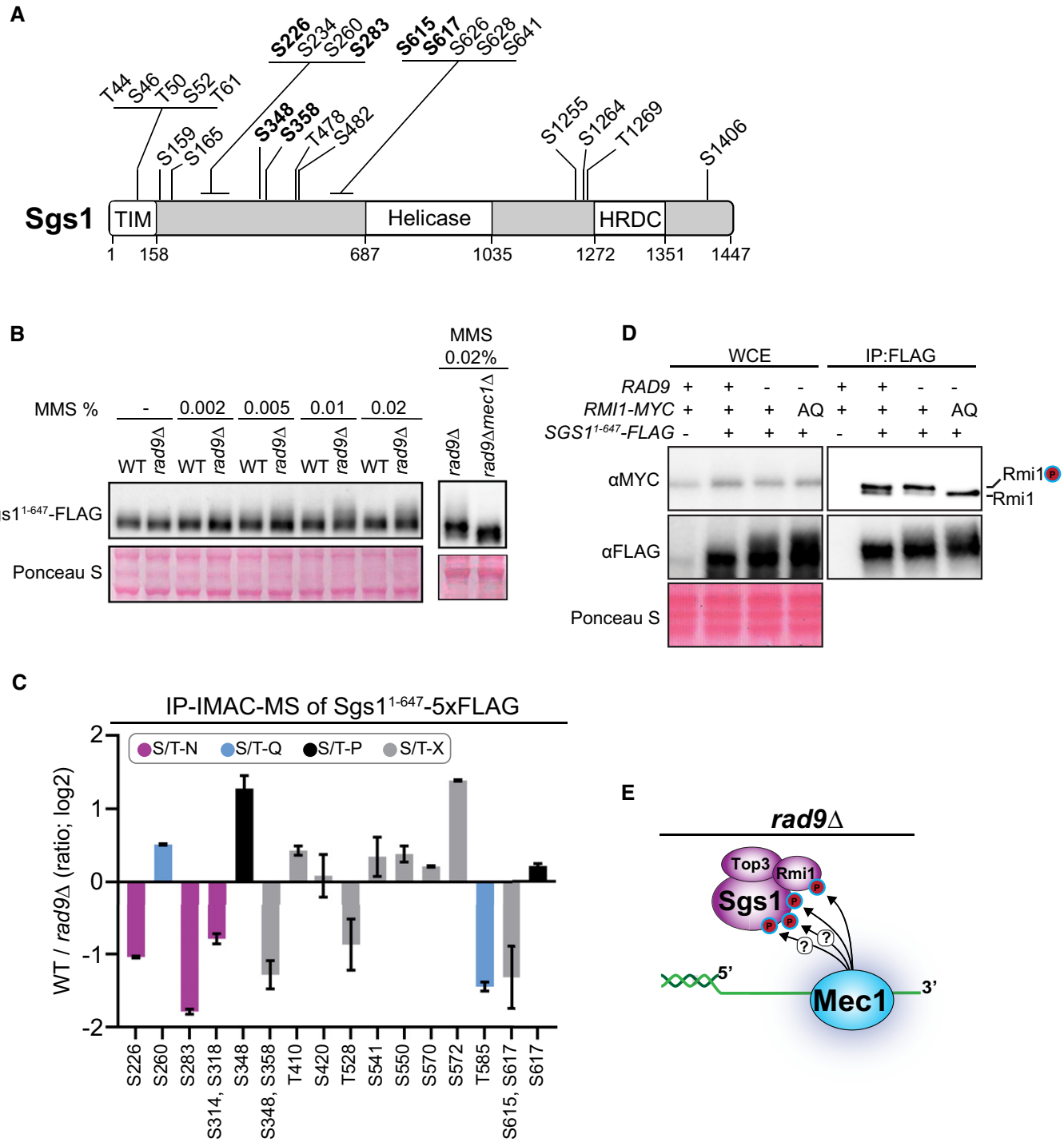

Figure 3.

Figure 3. The STR complex is phosphorylated at multiple sites in response to hyper-resection.

A Schematic representing all Sgs1 phosphorylation sites detected in a large scale, high coverage, phosphoproteomic dataset (Lanz *et al*, 2021). Bolded sites indicate those subsequently detected in the IP-MS phospho-mapping experiment in Fig 3C. TIM, Top3 interacting motif; HRDC, helicase and RnaseD C-terminal domain.

B Immunoblot analysis of Sgs1 N-terminus (amino acids 1–647) from cells treated with increasing doses of the DNA alkylating drug MMS in the absence of Rad9 alone (left blot), or in the absence of Rad9 and Mec1 (right blot). This truncated Sgs1 protein was expressed from its native promoter in this and all subsequent experiments.

C Quantitative mass spectrometry analysis of phosphopeptides from affinity-purified Sgs1 N-terminal fragment expressed in *rad9*Δ or wild-type 0.02% MMS-treated cells. Error bars represent standard deviation of two or more independent peptide-spectrum matches (PSMs) corresponding to the indicated sites.

D Rmi1, a component of the Sgs1-Top3-Rmi1 (STR) complex, is hyperphosphorylated on S/T-Q motifs in *rad9*Δ cells.

E Model for Mec1-dependent phosphorylation of the STR complex. For simplicity, the ssDNA-binding heterotrimer RPA and the obligatory Mec1 cofactor Ddc2 have been omitted from the diagram.

Source data are available online for this figure.

an intricate pattern of Mec1-dependent multi-phosphorylation of the STR complex in cells lacking Rad9, which likely involves additional downstream kinases (Fig 3E).

Sgs1 binds to the Dpb11 scaffold in cells lacking Rad9

Since the phosphorylation of Sgs1 by Mec1 was dependent on Ddc1-mediated Mec1 activation, we reasoned that Sgs1 might be brought in proximity to Mec1 through binding to Dpb11, a scaffolding protein that interacts with Ddc1 and has been previously reported to recruit known Mec1 targets, such as Slx4 and Rad9, to sites of DNA damage (Ohouo *et al,* 2010; Pfander & Diffley, 2011). We affinity-purified Dpb11 overexpressed in wild-type or *rad9*Δ cell lines and used mass spectrometry to identify interacting partners (Fig 4A–C and Dataset EV4). Expectedly, known Dpb11 interacting partners such as Ddc1, Sld2, Rtt107, and Slx4 co-purified with Dpb11 regardless of the status of Rad9. By contrast, Sgs1 and Top3, components of the STR complex, co-purified with Dpb11 only when *RAD9* was deleted (Fig 4C and D). To narrow down the region of Sgs1 that was responsible for binding to Dpb11, we tested whether the N-terminus of Sgs1 (amino acids 1–647; Fig 4E), previously shown to mediate various protein–protein interactions (Bjergbaek *et al,* 2005; Chiolo *et al,* 2005; Hegnauer *et al,* 2012), could bind to Dpb11. As with the full-length protein, the N-terminal 647 residues of Sgs1 pulled down Dpb11 in cells lacking the checkpoint adaptor Rad9, but the interaction was barely detectable when Rad9 was present (Fig 4F). Notably, the N-terminal 647 amino acid fragment of Sgs1 fused to a 5× FLAG tag was more stable than full-length Sgs1, and more amenable to our co-immunoprecipitation (Co-IP) experiments. Taken together, these findings uncover a previously undescribed interaction between Sgs1 and the Dpb11 scaffold and suggest a model whereby, in *rad9*Δ cells, Dpb11 bound to Ddc1 recruits the STR complex in proximity to Mec1 (Fig 4G).

Requirements for assembly of the Dpb11-STR complex

Next, we investigated the architecture of the Dpb11-Sgs1 interaction using a combination of quantitative affinity purification mass spectrometry (AP or IP-MS) and conventional Co-IP. To guide these experiments, we used the Dpb11-Rad9 and Dpb11-Slx4 interaction architecture as a model. In these complexes, Dpb11 binds to phosphorylated threonine 602 (pT602) on the Ddc1 subunit of the 9-1-1 clamp via Dpb11 BRCT domains 3 and 4. Ddc1 T602 phosphorylation is Mec1-dependent (Puddu *et al,* 2008), and upon engagement of the C-terminal BRCT domains of Dpb11 with the 9-1-1 clamp, the pair of N-terminal BRCTs (1 and 2) is free to engage phosphorylated interacting partners such as Rad9 and Slx4 (Pfander & Diffley, 2011; Cussiol *et al,* 2015).

Like the Dpb11-Rad9 and Dpb11-Slx4 complexes, the Dpb11-Sgs1 interaction was at least partially dependent on the N-terminal pair of BRCT domains in Dpb11, as evidenced by the reduction in interaction observed when the Dpb11-K55A mutant [which partially impairs BRCT 1, and binding via BRCT1/2 (Cussiol *et al,* 2015)] was used in the co-affinity purifications followed by MS analysis (Fig 5A and Dataset EV5). This result was corroborated by analysis of the $Dpb11^{K55A}$ mutant by Co-IP and western blot (Fig 5B). The partial phenotype of the BRCT1 mutant may be due to the nature of the mutant itself (i.e., it is not a full disruption of BRCT phosphopeptide-binding capability) or due to the complexity of the Dpb11-Sgs1 interaction, such as the potential involvement of additional Dpb11 domains. Expectedly, our mass spectrometry experiment also confirmed that the Dpb11-Slx4 interaction was dependent on functional

Figure 4. Sgs1 Interacts with the Dpb11 scaffold in *rad9*Δ cells.

A Workflow of the SILAC quantitative mass spectrometry method used to identify Dpb11 interacting proteins.

B Identification of Dpb11 interacting proteins in wild-type cells using workflow shown in (A). *DPB11-3xHA* was overexpressed using the *ADH1* promoter. *P* value calculated using Mann–Whitney *U*-test. Cells were grown in the presence of 0.04% MMS for 2 h.

C Identification of Dpb11-interacting proteins in *rad9*Δ cells using workflow shown in (A). *DPB11-3xHA* was overexpressed using the *ADH1* promoter. *P* value calculated using the Mann–Whitney *U*-test. Cells were grown in the presence of 0.04% MMS for 2 h.

D Immunoblot showing co-immunoprecipitation between Dpb11 and Sgs1. *DPB11-3xHA* was overexpressed from an *ADH1* promoter, and *SGS1-13xMYC* was expressed from its endogenous locus. In this and all subsequent Co-IP western blot experiments, cells were treated with 0.04% MMS for 2 h.

E Schematic of the Sgs1 N-terminal truncation used in this study.

F Immunoblot showing co-immunoprecipitation of Dpb11 with Sgs1. Both *DPB11-3xHA* and $SGS1^{1–647}$*-5xFLAG* were expressed at their endogenous loci.

G Hypothetical depiction of the Dpb11-STR complex engaged at 5' recessed ends. For simplicity, the ssDNA-binding heterotrimer RPA and the obligatory Mec1 cofactor Ddc2 have been omitted from the diagram.

Source data are available online for this figure.

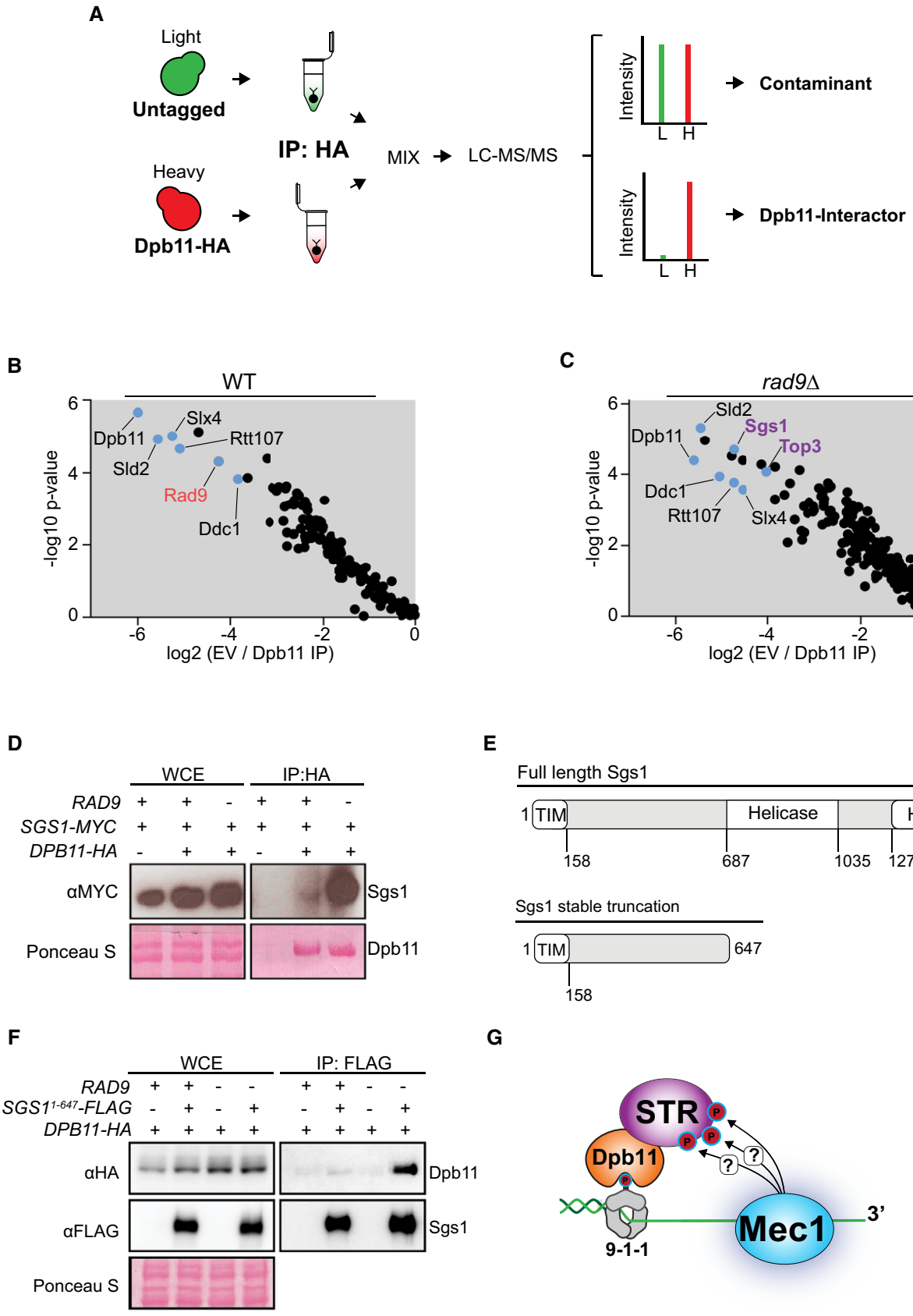

Figure 4.

N-terminal BRCT domains of Dpb11 (Cussiol *et al,* 2015). In addition, the Sld2-Dpb11 interaction, which is important for DNA replication initiation (Kamimura *et al,* 1998) and has been previously reported to depend on the C-terminal BRCT domains of Dpb11 (Tak *et al,* 2006), was not disrupted in binding to the $Dpb11^{K55A}$ protein (Fig 5A). The interaction of Dpb11 with the Mus81-Mms4 complex was also not disrupted in the K55A mutant. Of importance, the formation of the Dpb11-Sgs1 complex was also dependent on the 9-1-1 subunit Ddc1 and, specifically, on its phosphorylation by Mec1 at threonine 602 (Fig 5C and D, and Dataset EV5). Congruent with the requirement for Mec1, the deletion of *MEC1* also impaired the Dpb11-Sgs1 interaction, while the deletion of *TEL1* had no effect (Fig 5E and F, and Dataset EV5). These findings, together with our previous knowledge of how Dpb11 engages with the 9-1-1 complex, support a model in which Dpb11 engaged with the 9-1-1 clamp subunit Ddc1, via recognition of phosphorylated threonine 602 by BRCT3/4, interacts with the STR complex at least partially via BRCT1/2 of Dpb11 (Fig 6A). Since both Dpb11 and Ddc1 are established activators of Mec1, the initial engagement of STR with Dpb11 may further promote the extensive multi-site pattern of STR phosphorylation by Mec1. Strikingly, the architecture of the complex and its requirement for assembly are mostly similar to what was previously reported for the Dpb11-Slx4 interaction (Ohouo *et al,* 2010; Cussiol *et al,* 2015).

Generation of a BRCT-Sgs1 chimeric protein for functional interrogation of the Dpb11-Sgs1 interaction

As shown in Fig 6A, we hypothesized that Dpb11 is important to recruit or stabilize the STR complex at DNA lesions where a loaded 9-1-1 clamp is present, allowing STR to access intermediate DNA structures formed upon the overexposure of ssDNA. To test this model and gain insights into the role of the Dpb11-Sgs1 interaction, we fused full-length Sgs1 to BRCT domains 3 and 4 (B3/4) of Dpb11. As shown in Fig 6B, we reasoned that this chimeric protein should promote the enhanced recruitment of STR to the 9-1-1 clamp, bypassing the need for Mec1 to promote assembly of an Dpb11-Sgs1 complex, while still relying on phosphorylation of threonine 602 in Ddc1. Expression of B3/4-Sgs1 resulted in strong sensitivity to MMS in WT cells (Fig 6C), indicating that this chimeric protein exerts a dominant effect even in cells expressing Rad9. The MMS sensitivity was rescued by deletion of *DDC1* or by mutation of Ddc1 residue T602 to alanine, consistent with the model that the 9-1-1 clamp stabilizes STR at DNA lesions, which, in the case of the chimeric protein, may hyper-stabilize STR leading to aberrant control of the DNA damage response. Since Sgs1 has been reported to promote Rad53 activation in response to replication stress (Hegnauer *et al,* 2012), we monitored whether the B3/4-Sgs1 chimera impacted DNA damage checkpoint signaling. We did not observe a change in Rad53 activation in response to MMS treatment in cells expressing the chimeric protein (Fig 6D), suggesting that a B3/4-Sgs1 fusion protein impacts the DNA damage response independently of Rad53 activation. The STR complex plays major roles in the control of homologous recombination, including the surveillance of recombination intermediates and rejection of heteroduplexes to prevent non-allelic recombination (Chiolo *et al,* 2005; Lo *et al,* 2006; Ashton *et al,* 2011; Mirzaei *et al,* 2011; Klein & Symington, 2012; Bermúdez-López *et al,* 2016; Campos-Doerfler *et al,* 2018). Indeed, a major DNA repair pathway mediating MMS resistance is homologous recombination (Game & Mortimer, 1974). One explanation for the MMS sensitivity observed upon B3/4-Sgs1 expression could be that it is hyper-stabilizing the STR complex at DNA lesions, which is then rejecting recombination intermediates and not allowing execution of HR-mediated DNA repair of MMS-induced lesions. Consistent with this model, the expression of B3/4-Sgs1 resulted in extreme MMS sensitivity in cells lacking Rev3, a translesion synthesis factor (Fig 6E), which represents a pathway parallel to HR for the repair of MMS-induced DNA lesions (Doles *et al,* 2010; Jansen *et al,* 2015). These results support the model that Dpb11 stabilizes the STR complex at DNA lesions via the 9-1-1 clamp, which allows STR to engage recombination intermediates.

The B3/4-Sgs1 chimera impairs homology-directed repair

To determine whether the B3/4-Sgs1 fusion protein influences recombination outcomes, we used two well-established recombination assays for monitoring break-induced replication (BIR) or gene conversion (GC) (Fig 7A; Ira *et al,* 2003; Anand *et al,* 2014). The expression of B3/4-Sgs1 severely impaired break-induced replication (Fig 7B). The BIR defect was partially rescued by mutations that either impair helicase activity of Sgs1 (*hd*, helicase-defective mutation, $SGS1^{K706A}$) or impair the ability of Sgs1 to bind to Top3 (*tim*,

Figure 5. Requirements for assembly of the Dpb11-STR complex.

A Quantitative mass spectrometry analysis of affinity-purified Dpb11 complexes, comparing wild-type Dpb11 to the K55A mutant that partially impairs binding through BRCT domain 1. Cells were grown in the presence of 0.04% MMS. Error bars represent SEM of selected proteins for which there were 2 or more peptide-spectrum matches (PSMs).

B Immunoblots showing co-immunoprecipitation between Dpb11 and Sgs1 in the presence of 0.04% MMS in cells expressing either wild-type or the $DPB11^{K55A}$ mutant. *DPB11-3HA* or the BRCT mutant was ectopically expressed from its endogenous promoter and co-immunoprecipitated with $SGS1^{1-647}$-*FLAG* expressed from its endogenous promoter.

C Quantitative mass spectrometry analysis of affinity-purified Dpb11 complexes, comparing Dpb11 purified from *rad9*Δ cells with or without the 9-1-1 subunit Ddc1. Cells were grown in the presence of 0.04% MMS. Error bars represent SEM of selected proteins for which there were 2 or more peptide-spectrum matches (PSMs).

D Immunoblots showing co-immunoprecipitation between Dpb11 and Sgs1 in the presence of 0.04% MMS in either wild-type, *ddc1*Δ, or *ddc1-T602A* cell lines. *DPB11-3HA* was tagged at its endogenous locus and co-immunoprecipitated with $SGS1^{1-647}$-*FLAG* tagged and truncated at its endogenous locus.

E Quantitative mass spectrometry analysis of affinity-purified Dpb11 complexes, comparing Dpb11 purified from *rad9*Δ cells with or without Mec1. Cells were grown in the presence of 0.04% MMS. Error bars represent SEM of selected proteins for which there were 2 or more peptide-spectrum matches (PSMs).

F Immunoblots showing co-immunoprecipitation between Dpb11 and Sgs1 in the presence of 0.04% MMS in either wild-type, *mec1*Δ, *tel1*Δ, or *mec1*Δ *tel1*Δ cell lines. *DPB11-3HA* was tagged at its endogenous locus and co-immunoprecipitated with $SGS1^{1-647}$-*FLAG* tagged and truncated at its endogenous locus.

Source data are available online for this figure.

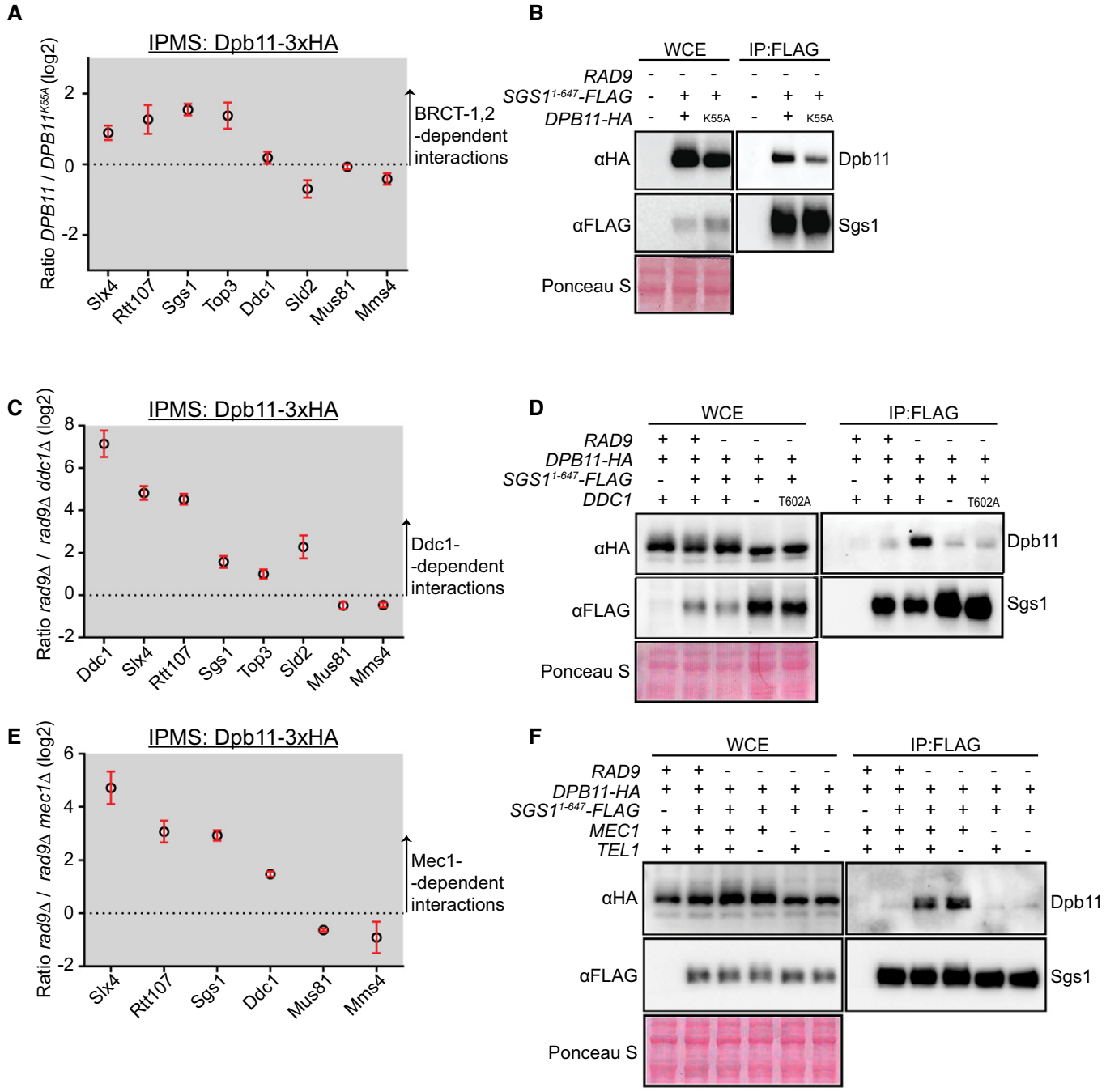

Figure 5.

top3 interacting motif, $SGS1^{\Delta 1-158}$) (Fig 7B), consistent with Sgs1's helicase activity and its Top3-binding capacity working cooperatively in D-loop dissociation (Piazza *et al,* 2019). A double *hd + TIM* mutant fully rescued the BIR defect of the chimera (Fig 7B). Fusing any of the three components of the STR complex to Dpb11 BRCT 3/4 impaired BIR to a similar extent (Fig 7C). Fusing other helicases such as Rrm3 or Pif1 to Dpb11 BRCT 3/4 did not significantly impair BIR (Fig 7D). Notably, fusing *Homo sapiens* BLM to Dpb11 BRCT 3/4 did significantly impair BIR (Fig 7D). Similar results were observed using the GC assay (Fig 7E and F). Finally, we asked whether the B3/4-Dpb11 fusion protein increases the stringency in single-strand annealing DNA repair using a previously published SSA reporter assay (Fig 7G; Sugawara *et al,* 2004). An increased SSA stringency would be manifested in this assay as a higher ratio of AA repair efficiency to FA repair efficiency since the FA strain contains 3% sequence non-homology and is therefore increasingly subject to Sgs1-mediated heteroduplex rejection. Indeed, expression of the B3/4-Sgs1 fusion protein led to an overall decrease in repair by SSA, as well as the predicted increase in the ratio of AA to FA repair product (Fig 7H and I), consistent with the chimeric protein increasing heteroduplex rejection. Overall, the results support a model in which Dpb11 and the 9-1-1 clamp play an important role

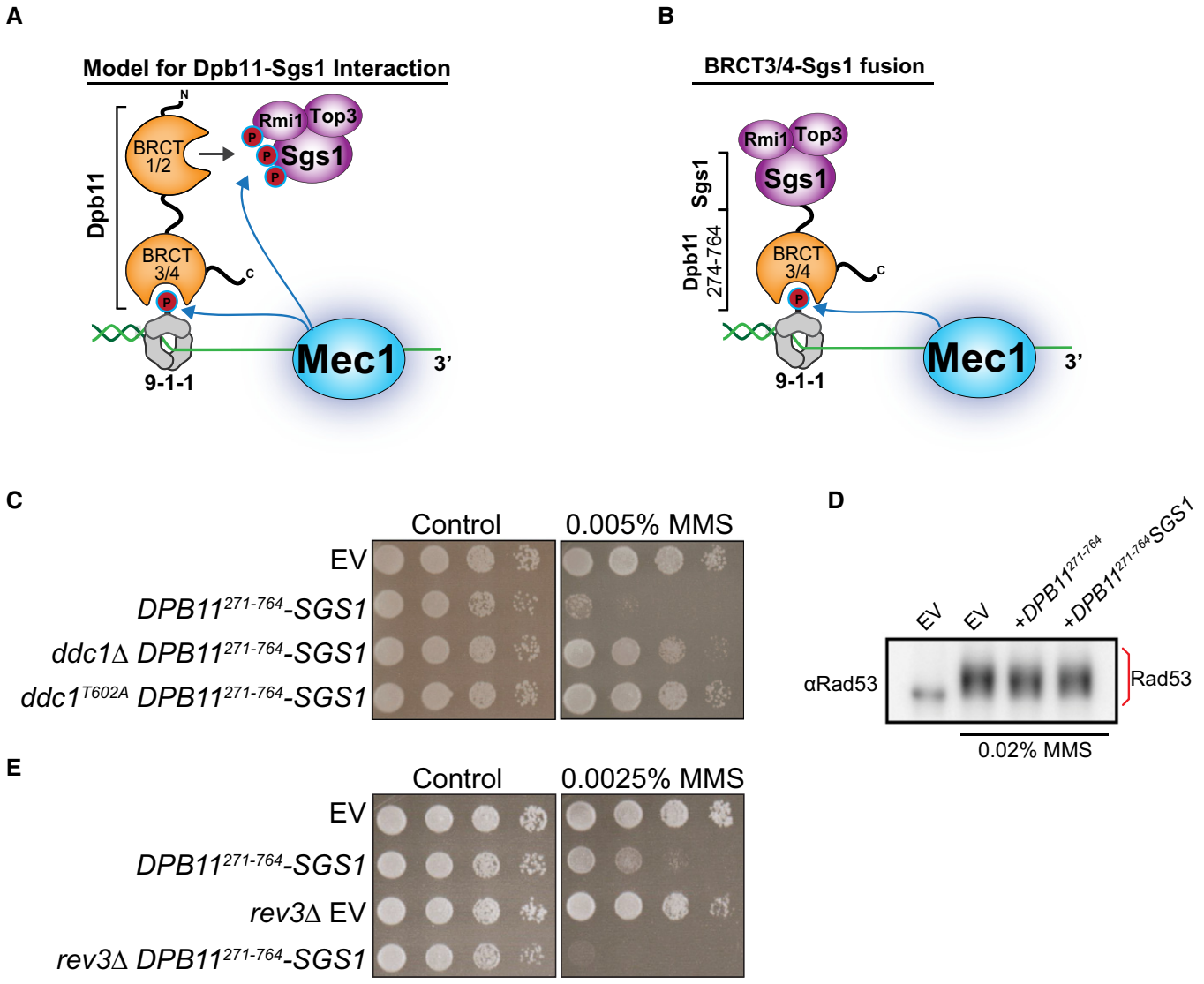

Figure 6. A BRCT-Sgs1 Fusion Protein Promotes MMS Sensitivity in a Ddc1-dependent Manner.

A, B Schematics depicting the rationale for designing a BRCT-Sgs1 chimera. The BRCT3/4-Sgs1 fusion protein is expected to engage at DNA lesions via the 9-1-1 clamp. For simplicity, the ssDNA-binding heterotrimer RPA and the obligatory Mec1 cofactor Ddc2 have been omitted from the diagram.

C Dilution assay of wild-type, *ddc1Δ*, or *ddc1-T602A* cells expressing *BRCT3/4-SGS1* in the presence of 0.005% MMS.

D Immunoblot of Rad53 mobility shift assay in cells treated with 0.02% MMS expressing either $DPB11^{BRCT3/4}$ alone or the *BRCT3/4-SGS1* chimera. Dilution assay of wild-type, *ddc1Δ*, or *ddc1-T602A* cells expressing *BRCT3/4-SGS1* in the presence of 0.005% MMS.

E Dilution assay of wild-type or *rev3Δ* cells expressing *BRCT3/4-SGS1* in the presence of 0.0025% MMS.

Source data are available online for this figure.

in controlling the action of STR. Since Mec1 mediates the interactions between Dpb11, Ddc1, and STR, our findings point to a role for Mec1 signaling in controlling recombination through the stabilization of STR at DNA lesions.

Impairing the Dpb11-Sgs1 interaction alters recombination outcomes

We sought to address the importance of the Dpb11-Sgs1 interaction for recombination outcomes by disrupting it. In search of minimal region(s) in Sgs1 critical for interaction with Dpb11, we expressed Sgs1 truncations lacking either one or both acidic patches in the N-terminus of Sgs1 (Fig 8A) and performed immunoprecipitation of Dpb11-HA followed by quantitative mass spectrometry analysis. As shown in Fig 8B, the region of Sgs1 most critical for interaction with Dpb11 was acidic patch 2 (AP2), located within the region of amino acids 502-647. Notably, this truncation displayed only modest MMS sensitivity (Fig 8C). To test the effect of the disrupted Dpb11-Sgs1 interaction on recombination-mediated DNA repair, we turned to the recent observation that the low BIR proficiency of cells lacking *RAD9* is partially rescuable by deletion of *SGS1* (Ferrari *et al,* 2020). We predicted that, if the Dpb11-Sgs1 interaction influences

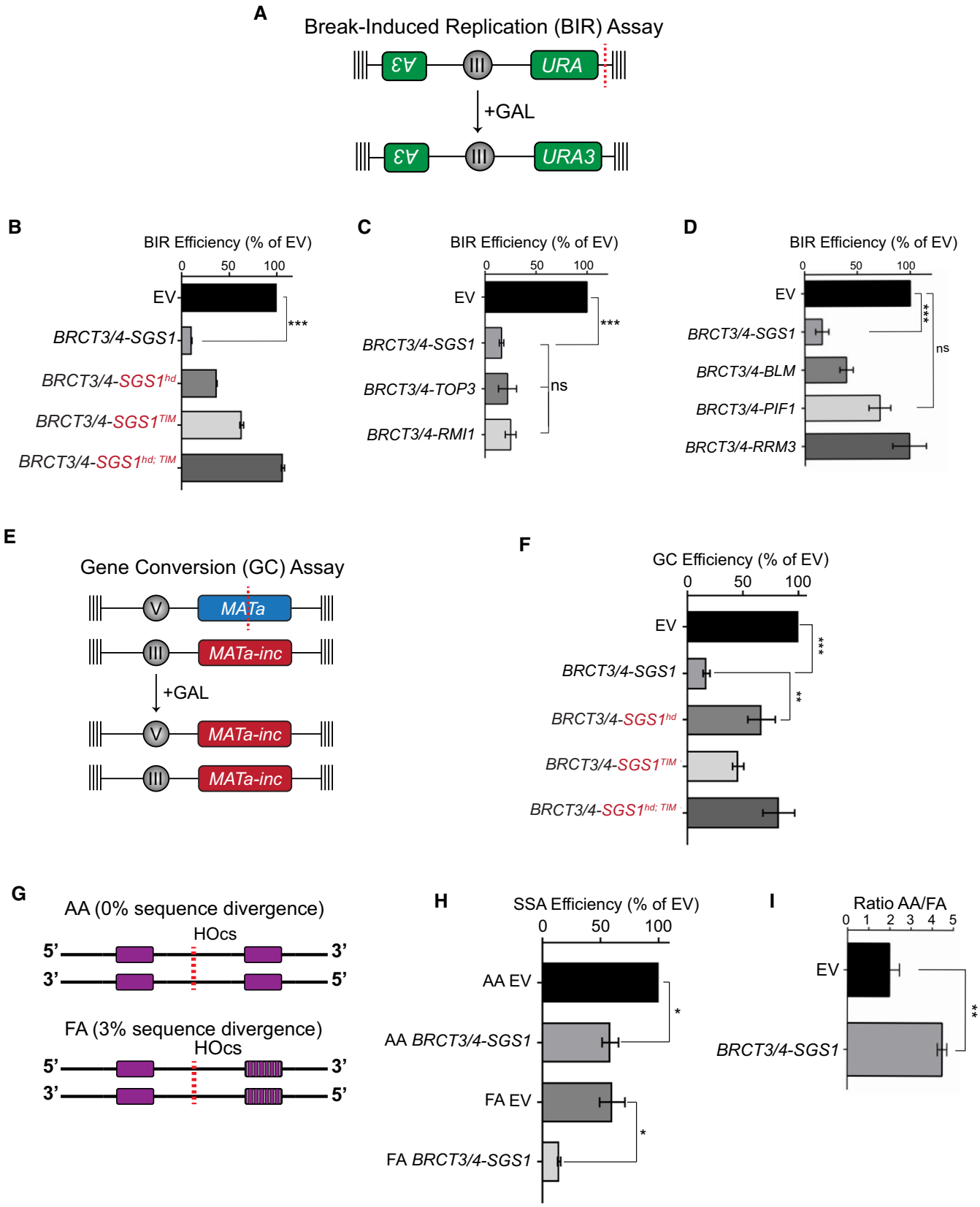

Figure 7.

Figure 7. The BRCT3/4-Sgs1 fusion protein impairs homologous recombination.

A Diagram of the break-induced replication (BIR) assay used in this study. Red line represents galactose-inducible HO endonuclease cut site.

B Measurement of BIR efficiency in cells carrying an empty vector or expressing *DPB11*$^{BRCT3/4}$ fused to wild-type or mutant versions of *SGS1*. Mutants include a helicase-deficient allele of *SGS1* (*SGS1*^{hd}) or an allele lacking the Top3 interacting motif (TIM; *SGS1*^{TIM}). Error bars represent SEM of at least 3 replicate experiments. *P* value was calculated with a two-tailed, unpaired *t*-test. **P* ≤ 0.05; ***P* ≤ 0.01; ****P* ≤ 0.001.

C Measurement of BIR efficiency in cells carrying an empty vector or expressing *DPB11*$^{BRCT3/4}$ fused to either *SGS1*, *TOP3*, or *RMI1*. Error bars represent SEM of at least 3 replicate experiments. *P* value was calculated with a two-tailed, unpaired *t*-test. **P* ≤ 0.05; ***P* ≤ 0.01; ****P* ≤ 0.001.

D Measurement of BIR efficiency in cells carrying an empty vector or *DPB11*$^{BRCT3/4}$ fused to either *SGS1*, hBLM, *PIF1*, or *RRM3*. Error bars represent SEM of at least 3 replicate experiments. *P* value was calculated with a two-tailed, unpaired *t*-test. **P* ≤ 0.05; ***P* ≤ 0.01; ****P* ≤ 0.001.

E Diagram of the gene conversion (GC) assay used in this study. Red line represents galactose-inducible HO endonuclease cut site.

F Measurement of gene conversion efficiency in cells carrying an empty vector or expressing *DPB11*$^{BRCT3/4}$ fused to wild-type or mutant versions of *SGS1*. Mutants include a helicase-deficient allele of *SGS1* (*SGS1*^{hd}) or an allele lacking the critical amino acid residues responsible for binding to Top3 (*SGS1*^{TIM}). Error bars represent SEM of at least 3 replicate experiments. *P* value was calculated with a two-tailed, unpaired *t*-test. **P* ≤ 0.05; ***P* ≤ 0.01; ****P* ≤ 0.001.

G Diagram of the single-strand annealing (SSA) assay used in this study. Red line represents galactose-inducible HO endonuclease cut site.

H Measurement of single-strand annealing in cells carrying an empty vector or expressing *DPB11*$^{BRCT3/4}$. Error bars represent SEM of at least 3 replicate experiments. AA strain contains perfect homology on either side of a GAL-inducible break. FA strain contains 3% sequence divergence on either side of the break (homeologous product).

I Ratio AA/FA repair product computed from data in (H). Error bars represent SEM of at least 3 replicate experiments. *P* value was calculated with a two-tailed, unpaired *t*-test. **P* ≤ 0.05; ***P* ≤ 0.01; ****P* ≤ 0.001.

recombination outcomes, then cells bearing *SGS1* alleles lacking acidic patch 2 would have elevated BIR proficiency relative to *rad9*Δ cells. Indeed, Sgs1 acidic patch mutants displayed elevated BIR proficiency over a *rad9*Δ cell line (Fig 8D). Taken together with results obtained using Dpb11-Sgs1 protein fusions, these data support the model that the Mec1-dependent Dpb11-Sgs1 interaction regulates recombination outcomes.

Discussion

Accumulated evidence over the past 30 years has identified Mec1 as a central player in the preservation of genome stability, particularly through the regulation of distinct steps of HR such as DNA end resection (Lanz *et al,* 2019). The precise mechanisms and targets regulated by Mec1 signaling for ensuring proper HR control remain incompletely understood, representing an important knowledge gap in our understanding of genome maintenance mechanisms. In this work, we sought to identify novel connections between Mec1/ATR signaling and the homologous recombination machinery. Using *rad9*Δ cells, we aimed to analyze a condition in which DNA lesions become hyper-resected and HR is dysregulated at a key early step. We reasoned that extensive ssDNA accumulation should increase the representation of recombination intermediates and Mec1-dependent signaling events important for HR control that are often too transient in wild-type cells. Consistent with the extensive processing of DNA ends in *rad9*Δ cells, our phosphoproteomic results revealed that in these cells Mec1/ATR preferentially targets proteins involved in ssDNA-associated transactions, including Rfa2, Uls1, and Sgs1. Therefore, the use of *rad9*Δ cells and quantitative MS analysis of phosphosignaling events allowed us to capture a distinctive Mec1/ATR signaling response that is likely under-represented in wild-type cells. We propose that this Mec1/ATR signaling is important to control HR-mediated repair events. Taken together, the identification of a distinct Mec1 signaling response triggered by hyper-resection highlights the multi-faceted action of this kinase in the coordination of checkpoint signaling and HR-mediated DNA repair (see model in Fig 9).

In addition to identifying Mec1/ATR signaling triggered by hyper-resection, our work finds that such signaling converges toward the assembly of a novel protein complex between the STR complex and the Dpb11 scaffold. In *rad9*Δ cells, Mec1/ATR phosphorylates the STR subunit Sgs1. While we find Mec1 signaling to be required for assembly of the STR-Dpb11, several details of how the multi-phosphorylation pattern in Sgs1 contributes to the interaction with Dpb11 remain incompletely understood. The available data suggest that the critical Dpb11 interaction domain resides in acidic patch 2 of Sgs1, a region previously shown to mediate an interaction between Sgs1 and RPA (Hegnauer *et al,* 2012). In the future, it will be important to identify the exact Sgs1 phosphorylation site(s) responsible for mediating its interaction with Dpb11. Alternatively, phosphorylation of any S/T-Q residue on Sgs1, Top3, or Rmi1 may be sufficient to induce the formation of STR-Dpb11 complexes. It also remains possible that phosphorylation of Ddc1 threonine 602 is the key Mec1-dependent phosphorylation important for mediating the Dpb11-Sgs1 interaction. In this scenario, the extensive exposure of ssDNA may promote the selective recruitment of STR complex close to Dpb11-9-1-1 complex, which is then recognized by BRCT1/2 of Dpb11 in a phosphorylation-independent manner. We do not favor this model, since BRCT1/2 of Dpb11 is well known to interact with phosphorylated epitopes (Bork *et al,* 1997; Yu *et al,* 2003; Pfander & Diffley, 2011; Cussiol *et al,* 2015). Of importance, we do not exclude the possibility that most of the Mec1-dependent phosphorylation events in Sgs1 are not involved in mediating the interaction with Dpb11, and that those may regulate additional aspects of Sgs1 function, such as conformational changes that alter its activity or ability to interact with other proteins.

Sgs1 is a well-established regulator of both early and later stages of homology-directed repair (Ira *et al,* 2003; Sugawara *et al,* 2004; Zhu *et al,* 2008; Mankouri *et al,* 2011). Sgs1 has well-defined roles in monitoring and disassembling recombination intermediates, including recombination-driven heteroduplexes (Cejka *et al,* 2012). Therefore, our findings suggested the model that upon hyper-resection of DNA ends, Mec1/ATR signaling converges to Sgs1 (and STR complex) as part of a quality control mechanism to prevent the aberrant exposure of ssDNA triggering erroneous HR events. Although alternative models remain plausible, the finding that the BRCT3/4-Sgs1

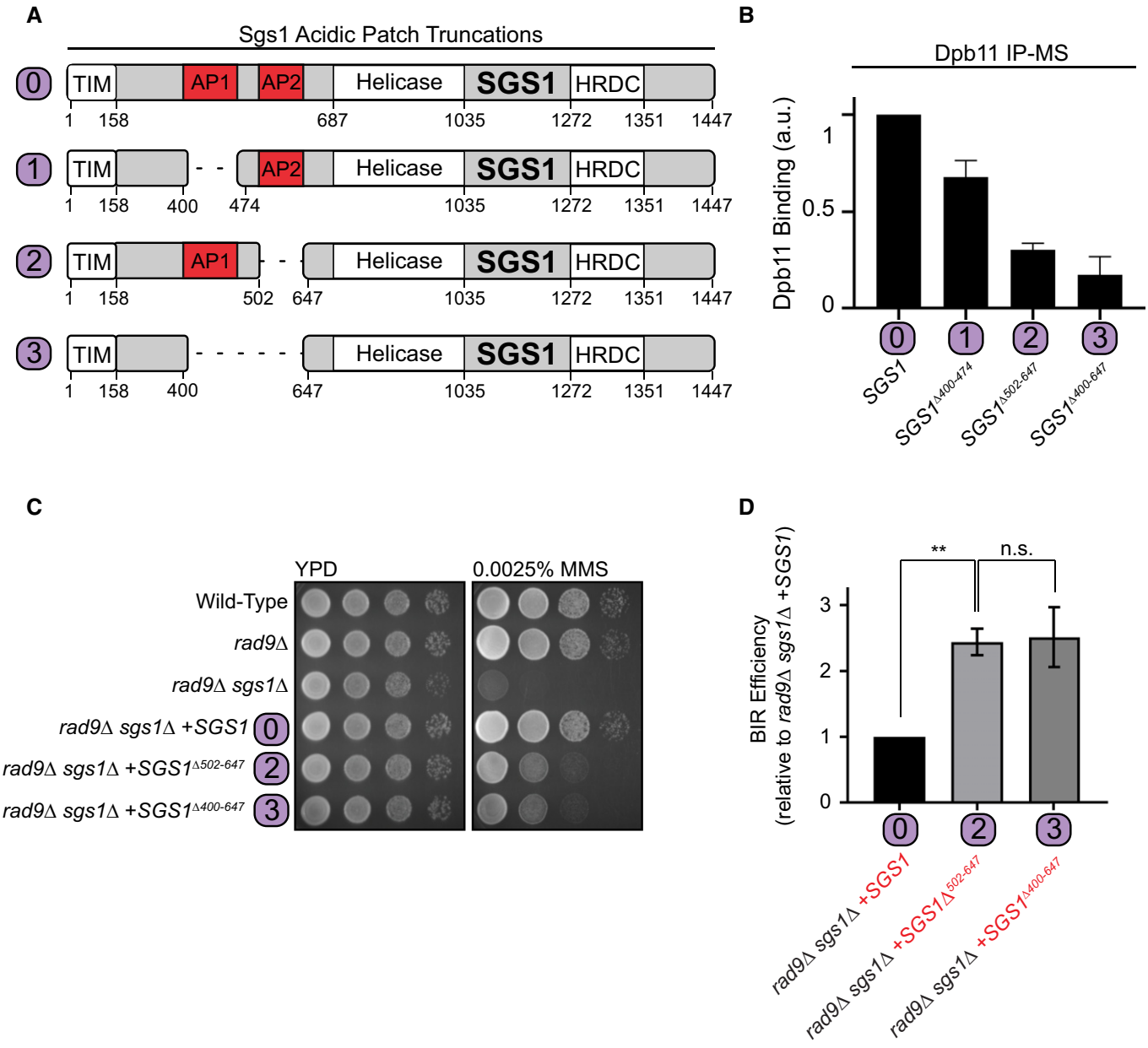

Figure 8. Disruption of the Dpb11-Sgs1 interaction modulates recombination outcomes.

A Diagram of the Sgs1 acidic patch (AP) truncations used in this study.

B Histogram showing abundance of Sgs1 peptides in Dpb11-HA co-immunoprecipitation mass spectrometry experiments from cells expressing either *SGS1* acidic patch truncation mutants or wild-type *SGS1*. Each mutant was compared in a SILAC experiment against the wild-type control. Error bars represent SEM of 2 or more Sgs1 peptide-spectrum matches (PSMs).

C Serial dilution assay of *sgs1Δ* cell lines expressing either *SGS1* or *sgs1*$^{\Delta ACIDICPATCH}$.

D BIR assay in *rad9Δ sgs1Δ* cell lines expressing either *SGS1* or *sgs1*$^{\Delta ACIDICPATCH}$. Error bars represent SEM of 3 independent experiments. *P* value was calculated with a two-tailed, unpaired *t*-test. *$P \leq 0.05$; **$P \leq 0.01$; ***$P \leq 0.001$.

fusion protein impairs HR-mediated repair supports the quality control model. Of importance, this fusion did not alter Rad53 signaling, consistent with the notion that the chimera does not interfere with checkpoint signaling. Since Rad53 signaling is often tightly correlated with the extent of resection, this finding suggests that resection is not affected by expression of the B3/4-Sgs1 chimera. This is not surprising, since Sgs1 requires Dna2 in its function of promoting long-range resection (Zhu *et al*, 2008). As such, the results corroborate our model of the chimera impairing heteroduplex stability and preventing recombination events. That the chimeric protein is capable of inhibiting HR-mediated repair via single-strand annealing, which does

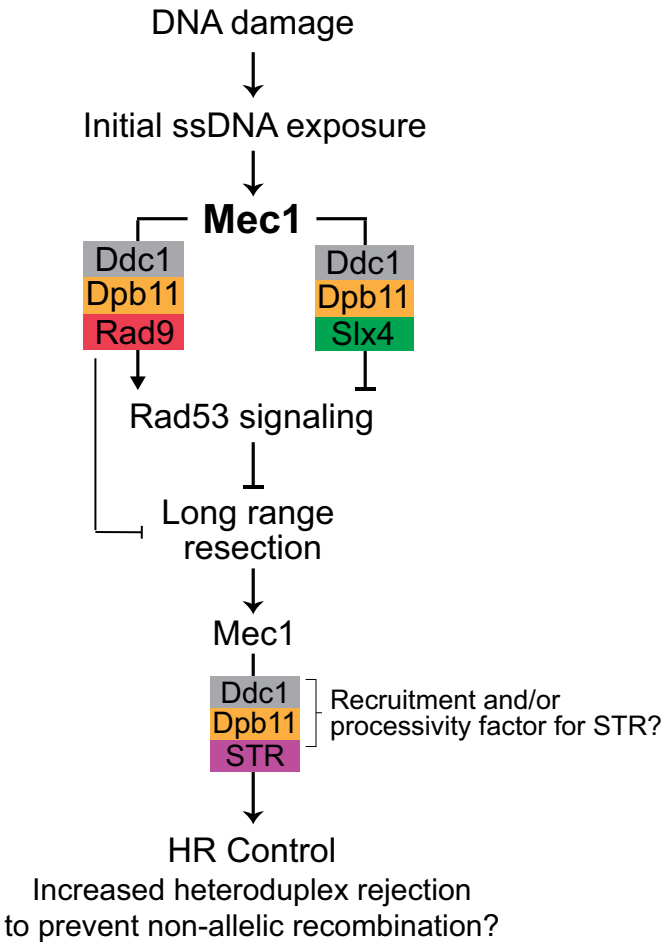

Figure 9. Model for distinct modes of Mec1 signaling in the control of checkpoint signaling and homologous recombination.

Mec1 is recruited to RPA-ssDNA following DNA damage to promote Rad53-mediated checkpoint signaling that prevents immediate long-range resection of DNA ends. This anti-resection function of Mec1 is important to protect DNA ends and ensure that subsequent resection occurs in a controlled fashion. Since the Dpb11-Rad9 interaction is not dependent on Mec1 (but mostly dependent on CDK phosphorylation), the Dpb11-Rad9 complex is rapidly stabilized at DNA lesions once initial Mec1 signaling and Ddc1 phosphorylation occurs. As Mec1 signaling builds, it phosphorylates the Slx4 scaffold, which becomes a strong interactor of Dpb11 and displaces Rad9 to counteract checkpoint signaling and Rad9-mediated resection inhibition. It is at this point that Mec1 signaling switches to an anti-checkpoint and pro-resection mode. Once long-range resection occurs, extensive ssDNA accumulates, leading to increased opportunities for strand invasion, but also increased opportunities for non-allelic recombination (*rad9*Δ cells have increased non-allelic recombination (Fasullo *et al*, 1998; Nielsen *et al*, 2013). In this context, we propose that a new mode of Mec1 signaling triggered by extensive resection stabilizes the STR complex at lesions via interaction with Dpb11 for proper regulation of HR. It is tempting to speculate that the Dpb11-9-1-1 complex acts as a "processivity factor" for the helicase function of Sgs1 to processively displace, and reject, heteroduplexes.

not involve the formation of joint molecules, supports a role for the Dpb11-Sgs1 interaction in quality control at stages of HR that precede the formation of joint molecules. Nonetheless, the possibility exists that the Dpb11-Sgs1 interaction could also play a role in regulating later steps of HR where Sgs1 is also known to function, such as the dissolution of double Holliday junctions.

Based on our finding that a BLM-B3/4 fusion protein robustly impairs recombination, it is tantalizing to speculate that the TOPBP1-BLM interaction in mammalian cells plays a similar role as *S. cerevisiae* Dpb11-Sgs1. Indeed, BLM and TOPBP1 are known to interact in human cells (Wang *et al*, ,2013, 2015; Blackford *et al*, 2015; Sun *et al*, 2017; Mer & Botuyan, 2017), although it is unclear whether ATR plays any role in promoting that interaction and whether the BLM-TOPBP1 interaction controls HR. What is clear is that ATR signaling in mammalian cells, similar to what we observed for Mec1 in budding yeast here, is channeled through different pathways depending on the context of the DNA lesion, including the extent of ssDNA exposure (Shiotani *et al*, 2013).

The discovery of the Dpb11-STR complex and its mode of interaction and engagement with the 9-1-1 complex reveals an important additional role for Dpb11 in controlling the DNA damage response. Notably, the assembly of the complex and requirements for interaction follow a similar logic to what was previously reported for the Dpb11-Rad9 and Dpb11-Slx4-Rtt107 complexes, as well as the Dpb11-Fun30 interaction (Ohouo *et al*, 2010; Pfander & Diffley, 2011; Gritenaite *et al*, 2014; Cussiol *et al*, 2015; Bantele *et al*, 2017). Future work should focus on elucidating how the formation of the four independent Ddc1-dependent Dpb11 complexes (Dpb11-Fun30, Dpb11-Rad9, Dpb11-Sgs1, and Dpb11-Slx4) is spatiotemporally regulated. For example, it would be interesting to test whether Dpb11 interactors compete directly or instead bind discrete 9-1-1 complexes. Biochemical data suggest that 9-1-1 clamps, once loaded, can slide along plasmid DNA substrates, on both ssDNA and dsDNA (Majka & Burgers, 2003), raising the possibility that many 9-1-1 clamps could be loaded onto DNA per lesion, with each clamp harboring a Dpb11 molecule and its associated interacting partner, dependent perhaps on the sequence or structural context of the DNA. Future work may also reveal novel Mec1-dependent interactors of Dpb11, expanding on the common logic for how Mec1 coordinates the DNA damage response and cementing Dpb11 as a critical scaffolding protein that integrates Mec1 signaling inputs into the formation of concerted repair protein complex outputs.

The Mec1 signaling response we found induced by hyper-resection in cells lacking Rad9 likely plays additional important roles in DNA repair control besides modulating STR action. We also detected that lack of Rad9 induces the phosphorylation of Uls1, a ubiquitin ligase and DNA translocase, reported to control HR. While less is understood about Uls1 than Sgs1, genetic studies have linked Uls1 to Sgs1 through Uls1's translocase function, which may channel recombination intermediates into Sgs1-dependent repair mechanisms (Cal-Bkowska *et al*, 2011). Future work focused on the role of Mec1 phosphorylation of Uls1 may illuminate connections between Uls1, Sgs1, and Mec1, and potentially reveal novel mechanisms regulating recombination in response to hyper-resection. Interestingly, Uls1 did appear in our Dpb11 IP-MS experiments as a Dpb11 interactor in *rad9*Δ cells, but the number of peptides identified was too low to pass our threshold for calling Dpb11 interactors. While the impairment of resection control, as achieved here through the deletion of *RAD9*, allowed us to uncover a previously undescribed function for Mec1, future work based on mutants that impair other steps of HR may reveal additional roles for Mec1 in controlling multiple steps of HR.

Materials and Methods

Yeast strains

A complete list of yeast strains used in this study can be found in Table EV1. Whole ORF deletions were performed using the established PCR-based strategy to amplify resistance cassettes with flanking sequence homologous to a target gene (Longtine *et al,* 1998). The *dna2-aid* allele was constructed using a PCR-amplified *aid-6xFLAG-T_{CYC2}-hphNT* tagging cassette derived from pHyg-AID*-6FLAG (Morawska & Ulrich, 2013). All whole ORF deletions and epitope tags were verified by PCR. Primer sequences for gene deletions are available in Table EV2. Yeast strains were grown at 30°C in a shaker incubator at 220 rpm. For strains with integrated genetic modifications, YEPD media were used. For strains bearing plasmids, the requisite synthetic dropout media were used. Plasmids in this study are listed in Table EV3 and are available upon request. For SILAC experiments, yeast strains were grown in -Arg -Lys media supplemented with either isotopically normal arginine and lysine or the $^{13}C^{15}N$ isotopologue. Excess proline (to prevent conversion of arginine to proline) was added to SILAC media at a concentration of 80 mg/l.

Co-immunoprecipitation

Yeast cell lysates were prepared for immunoprecipitation by bead beating for three cycles of 10 min with 1-min rest between cycles at 4°C in lysis buffer (150 mM NaCl, 50 mM Tris pH 7.5, 5 mM EDTA, 0.2% Tergitol type NP-40) supplemented with complete EDTA-free protease inhibitor cocktail (Roche), 5 mM sodium fluoride, and 10 mM β-glycerophosphate. Following normalization by Bradford assay, ~ 5 mg of lysate per IP was incubated with antibody-conjugated agarose resin for 3 h at 4°C. Resin was washed 4× in lysis buffer. Elution was performed either with FLAG peptide or elution buffer (1% SDS, 100 mM Tris pH 8.0).

Immunoprecipitation–mass spectrometry (IP-MS)

For IP-MS experiments, control yeast or yeast expressing tagged bait proteins were grown in "heavy" or "light" SILAC media [complete synthetic medium -Arg-Lys supplemented with either isotopically heavy (containing ^{13}C and ^{15}N) or normal (containing ^{12}C and ^{14}N) lysine and arginine] to mid-log phase and treated as described in the figure legend. Cells were pelleted at 1,000 rcf and washed with TE buffer containing 1 mM PMSF. Pellets from "light" and "heavy" samples were lysed and processed separately as described for Co-IP above. Proteins bound to antibody-conjugated agarose resin were eluted with 1% SDS, 100 mM Tris pH 8.0, and then, "light" and "heavy" eluates were mixed, reduced with 10 mM DTT, and alkylated with 25 mM iodoacetamide followed by precipitation on ice for 1 h in PPT solution (50% acetone, 49.9% ethanol, 0.1% acetic acid). Pellets were washed once with PPT and then resuspended in urea/Tris solution (8 M urea, 50 mM Tris pH 8.0). Urea-solubilized pellet was then diluted to 2 M urea using NaCl/Tris solution (150 mM NaCl, 50 mM Tris pH 8.0) and digested overnight at 37°C with 10 μg of trypsin GOLD (Promega). The following day, samples were desalted using a 50 mg Waters Sep-Pak column. Eluted peptides were dried and resuspended in 0.1% TFA and subjected for LC-MS/MS analysis on a Thermo Fisher Q Exactive HF mass spectrometer as recently described (Lanz *et al,* 2018).

Phosphoproteomics

For phosphoproteomic experiments, 200 ml of yeast grown in "heavy" or "light" SILAC media [complete synthetic medium -Arg-Lys supplemented with isotopically heavy (containing ^{13}C and ^{15}N) or normal (containing ^{12}C and ^{14}N) lysine and arginine] to mid-log phase and treated as described in the figure legend. Cells were pelleted at 1,000 rcf and washed with TE buffer containing 1 mM PMSF. Pellets were lysed by bead beating with 0.5-mm glass beads for three cycles of 10 min with 1-min rest time between cycles at 4°C in lysis buffer (150 mM NaCl, 50 mM Tris pH 7.5, 5 mM EDTA, 0.2% Tergitol type NP-40) supplemented with complete EDTA-free protease inhibitor cocktail (Roche), 5 mM sodium fluoride, and 10 mM β-glycerophosphate. Seven mg of each light- and heavy-labeled protein lysate was denatured and reduced with 1% SDS and 5 mM DTT at 65°C, and then alkylated with 25 mM iodoacetamide. Light and heavy protein lysates were mixed and precipitated with a cold solution of 50% acetone, 49.9% ethanol, and 0.1% acetic acid. Protein pellet was resuspended with 2 M urea and subsequently digested with TPCK-treated trypsin overnight at 37°C. For the resection dependency experiment in Fig 2, TMT quantification was used instead of SILAC. The pipeline remained the same, except that lysates were not mixed until after labeling with the amine-reactive TMT reagent. Phosphoenrichment was performed using a Thermo Fisher Fe-NTA Phosphopeptide Enrichment Kit (cat# A32992) according to the manufacturer's protocol. Purified phosphopeptides were then fractionated using HILIC chromatography and subjected to LC-MS/MS on a Thermo Fisher Q Exactive HF mass spectrometer as recently described (Lanz *et al,* 2018).

Mass spectrometry data analysis

For IP/MS experiments, raw MS/MS spectra were searched using the SORCERER (Sage N Research, Inc.) system running the SEQUEST software over a composite yeast protein database, consisting of both the normal yeast protein sequences downloaded from the Saccharomyces Genome Database (SGD) and their reversed protein sequences as a decoy to estimate the false discovery rate (FDR) in the search results. Searching parameters included a semi-tryptic requirement, a mass accuracy of 15 ppm for the precursor ions, differential modification of 8.0142 daltons for lysine, 10.00827 daltons for arginine, and a static mass modification of 57.021465 daltons for alkylated cysteine residues. XPRESS software, part of the Trans-Proteomic Pipeline (Seattle Proteome Center), was used to quantify all the identified peptides. Proteins with fewer than 4 PSMs identified were excluded. Statistical analyses were performed using a Wilcoxon rank-sum test.

For phosphoproteomic experiments, raw MS/MS spectra were searched using the COMET engine (part of the Trans-Proteomic Pipeline; Seattle Proteome Center) over a composite yeast protein database, consisting of both the normal yeast protein sequences downloaded from the Saccharomyces Genome Database (SGD) and their reversed protein sequences as a decoy to estimate the false discovery rate (FDR) in the search results. Searching parameters included a semi-tryptic requirement, a mass accuracy of 15 ppm for

the precursor ions, differential modification of 8.0142 daltons for lysine, 10.00827 daltons for arginine, 79.966331 daltons for phosphorylation of serine, threonine, and tyrosine (for phosphoproteomic experiments) and a static mass modification of 57.021465 daltons for alkylated cysteine residues. Phosphorylation site localization probabilities were determined using PTMProphet, and quantitation of identified phosphopeptides was performed using XPRESS (both tools part of the Trans-Proteomic Pipeline; Seattle Proteome Center) for SILAC data or the libra package for TMT data (also part of the TPP). SILAC phosphoproteomic data shown in Figs 1 and 2 represent the combined independent results of a "forward" (condition 1 = light/condition 2 = heavy) and a "reverse" (condition 1 = heavy/condition 2 = light) SILAC experiment. Using this experimental design, phosphorylation events that were not consistently identified in two independent, separately SILAC-labeled yeast cultures, were filtered out, as previously described (Faca *et al*, 2020). All mass spectrometric data presented in this study are available through PRIDE (see data availability statement).

Western blots

Yeast cell lysates were prepared for western blotting by bead beating for 15 min at 4°C in lysis buffer (150 mM NaCl, 50 mM Tris pH 7.5, 5 mM EDTA, 0.2% Tergitol type NP-40) supplemented with complete EDTA-free protease inhibitor cocktail (Roche), 5 mM sodium fluoride, and 10 mM β-glycerophosphate. Following normalization by the Bradford assay, lysates were boiled in Laemmli buffer and electrophoresed on a 9% SDS–PAGE gel. Proteins were transferred wet onto a PVDF membrane and incubated with antibody. Signal detection was performed using HRP-coupled secondary antibodies in all cases, imaged either with a Bio-Rad ChemiDoc or with X-ray film.

Genetic assays to measure recombination

BIR assay was performed according to Anand *et al* (2014). GC assay was performed as described in Ira *et al* (2003). SSA assay was performed according to Sugawara *et al* (2004).

Spot assays

For dilution assays, 5 ml of yeast culture was grown to saturation at 30°C. Then, 1 OD600 equivalent of the saturated culture was 10-fold serially diluted in a 96-well plate in water and spotted onto agar plates using a bolt pinner.

Data availability

The mass spectrometry data from this publication have been deposited to the PRIDE database (https://www.ebi.ac.uk/pride/archive/) and assigned the identifiers PXD017286, PXD017289, and PXD023438.

Expanded View for this article is available online.

Acknowledgements
We thank Beatriz S. Almeida for technical support; we thank Jim Haber, Gregorz Ira, and Eric Alani for graciously providing yeast strains YRA213, TGI354, and EAY1141/54, respectively; we thank Xiaolan Zhao for careful reading of the manuscript and comments; and we thank Diego Dibitetto and other members of the Smolka Lab for valuable discussions related to this work. This work is supported by a grant from the National Institute of Health, R01 GM097272, to M.B.S, and R35 GM126997 to L.S.S.

Author contributions
EJS and MBS conceptualized the project, designed the experiments, interpreted data, and wrote the paper. EJS, SCV, and WJC performed experiments. VMF, EJS, WJC, and MBS designed the phosphoproteomic data analysis pipeline. RG and LSS constructed and validated the Dna2 conditional depletion strains.

Conflict of interest
The authors declare that they have no conflict of interest.

References

Anand RP, Tsaponina O, Greenwell PW, Lee CS, Du W, Petes TD, Haber JE (2014) Chromosome rearrangements via template switching between diverged repeated sequences. *Genes Dev* 28: 2394 – 2406

Ashton TM, Mankouri HW, Heidenblut A, McHugh PJ, Hickson ID (2011) Pathways for holliday junction processing during homologous recombination in *Saccharomyces cerevisiae*. *Mol Cell Biol* 31: 1921 – 1933

Bantele SCS, Ferreira P, Gritenaite D, Boos D, Pfander B (2017) Targeting of the Fun30 nucleosome remodeller by the Dpb11 scaffold facilitates cell cycle-regulated DNA end resection. *Elife* 6: e21687

Barlow JH, Rothstein R (2009) Rad52 recruitment is DNA replication independent and regulated by Cdc28 and the Mec1 kinase. *EMBO J* 28: 1121 – 1130

BastosdeOliveira FM, Kim D, Cussiol JR, Das J, Jeong MC, Doerfler L, Schmidt KH, Yu H, Smolka MB (2015) Phosphoproteomics reveals distinct modes of Mec1/ATR signaling during DNA replication. *Mol Cell* 57: 1124 – 1132

Bermúdez-López M, Villoria MT, Esteras M, Jarmuz A, Torres-Rosell J, Clemente-Blanco A, Aragon L (2016) Sgs1's roles in DNA end resection, HJ dissolution, and crossover suppression require a two-step SUMO regulation dependent on Smc5/6. *Genes Dev* 30: 1339 – 1356

Bjergbaek L, Cobb JA, Tsai-Pflugfelder M, Gasser SM (2005) Mechanistically distinct roles for Sgs1p in checkpoint activation and replication fork maintenance. *EMBO J* 24: 405 – 417

Blackford AN, Nieminuszczy J, Schwab RA, Galanty Y, Jackson SP, Niedzwiedz W (2015) TopBP1 interacts with BLM to maintain genome stability but is dispensable for preventing BLM degradation. *Mol Cell* 57: 1133 – 1141

Bork P, Hofmann K, Bucher P, Neuwald AF, Altschul SF, Koonin EV (1997) A superfamily of conserved domains in DNA damage- responsive cell cycle checkpoint proteins. *FASEB J* 11: 68 – 76

Cal-Bkowska M, Litwin I, Bocer T, Wysocki R, Dziadkowiec D (2011) The Swi2-Snf2-like protein Uls1 is involved in replication stress response. *Nucleic Acids Res* 39: 8765 – 8777

Campos-Doerfler L, Syed S, Schmidt KH (2018) Sgs1 binding to Rad51 stimulates homology-directed DNA repair in saccharomyces cerevisiae. *Genetics* 208: 125 – 138

Cejka P, Plank JL, Dombrowski CC, Kowalczykowski SC (2012) Decatenation of DNA by the *S. cerevisiae* Sgs1-Top3-Rmi1 and RPA complex: a mechanism for disentangling chromosomes. *Mol Cell* 47: 886 – 896

Cha RS, Kleckner N (2002) ATR homolog Mec1 promotes fork progression, thus averting breaks in replication slow zones. *Science* 297: 602 – 606

Chiolo I, Carotenuto W, Maffioletti G, Petrini JHJ, Foiani M, Liberi G (2005) Srs2 and Sgs1 DNA helicases associate with Mre11 in different subcomplexes following checkpoint activation and CDK1-mediated Srs2 phosphorylation. *Mol Cell Biol* 25: 5738 – 5751

Clerici M, Trovesi C, Galbiati A, Lucchini G, Longhese MP (2014) Mec1/ATR regulates the generation of single-stranded DNA that attenuates Tel1/ATM signaling at DNA ends. *EMBO J* 33: 198 – 216

Cussiol JR, Jablonowski CM, Yimit A, Brown GW, Smolka MB (2015) Dampening DNA damage checkpoint signalling via coordinated BRCT domain interactions. *EMBO J* 34: 1704 – 1717

Dayon L, Hainard A, Licker V, Turck N, Kuhn K, Hochstrasser DF, Burkhard PR, Sanchez JC (2008) Relative quantification of proteins in human cerebrospinal fluids by MS/MS using 6-plex isobaric tags. *Anal Chem* 80: 2921 – 2931

Desany BA, Alcasabas AA, Bachant JB, Elledge SJ (1998) Recovery from DNA replicational stress is the essential function of the S-phase checkpoint pathway. *Genes Dev* 12: 2956 – 2970

Deshpande I, Seeber A, Shimada K, Keusch JJ, Gut H, Gasser SM (2017) Structural basis of Mec1-Ddc2-RPA assembly and activation on single-stranded DNA at sites of damage. *Mol Cell* 68: 431 – 445.e5

Dibitetto D, Ferrari M, Rawal CC, Balint A, Kim T, Zhang Z, Smolka MB, Brown GW, Marini F, Pellicioli A (2015) Slx4 and Rtt107 control checkpoint signalling and DNA resection at double-strand breaks. *Nucleic Acids Res* 44: 669 – 682

Dion V, Kalck V, Horigome C, Towbin BD, Gasser SM (2012) Increased mobility of double-strand breaks requires Mec1, Rad9 and the homologous recombination machinery. *Nat Cell Biol* 14: 502 – 509

Doles J, Oliver TG, Cameron ER, Hsu G, Jacks T, Walker GC, Hemann MT (2010) Suppression of Rev3, the catalytic subunit of Pol?, sensitizes drug-resistant lung tumors to chemotherapy. *Proc Natl Acad Sci USA* 107: 20786 – 20791

Faca VM, Sanford EJ, Tieu J, Comstock W, Gupta S, Marshall S, Yu H, Smolka MB (2020) Maximized quantitative phosphoproteomics allows high confidence dissection of the DNA damage signaling network. *Sci Rep* 10: 308

Fasullo M, Bennett T, Ahching P, Koudelik J (1998) The *Saccharomyces cerevisiae* RAD9Checkpoint reduces the DNA damage-associated stimulation of directed translocations. *Mol Cell Biol* 18: 1190 – 1200

Ferrari M, Rawal CC, Lodovichi S, Vietri MY, Pellicioli A (2020) Rad9/53BP1 promotes DNA repair via crossover recombination by limiting the Sgs1 and Mph1 helicases. *Nat Commun* 11: 3181

Flott S, Kwon Y, Pigli YZ, Rice PA, Sung P, Jackson SP (2011) Regulation of Rad51 function by phosphorylation. *EMBO Rep* 12: 833 – 839

Game JC, Mortimer RK (1974) A genetic study of X-ray sensitive mutants in yeast. *Mutat Res* 24: 281 – 292

Gritenaite D, Princz LN, Szakal B, Bantele SCS, Wendeler L, Schilbach S, Habermann BH, Matos J, Lisby M, Branzei D *et al* (2014) A cell cycle-regulated Slx4-Dpb11 complex promotes the resolution of DNA repair intermediates linked to stalled replication. *Genes Dev* 28: 1604 – 1619

Han DK, Eng J, Zhou H, Aebersold R (2001) Quantitative profiling of differentiation-induced microsomal proteins using isotope-coded affinity tags and mass spectrometry. *Nat Biotechnol* 19: 946 – 951

Hegnauer AM, Hustedt N, Shimada K, Pike BL, Vogel M, Amsler P, Rubin SM, Van Leeuwen F, Guénolé A, Van Attikum H *et al* (2012) An N-terminal acidic region of Sgs1 interacts with Rpa70 and recruits Rad53 kinase to stalled forks. *EMBO J* 31: 3768 – 3783

Hogrebe A, Von Stechow L, Bekker-Jensen DB, Weinert BT, Kelstrup CD, Olsen JV (2018) Benchmarking common quantification strategies for large-scale phosphoproteomics. *Nat Commun* 9: 1045

Huang M, Zhou Z, Elledge SJ (1998) The DNA replication and damage checkpoint pathways induce transcription by inhibition of the Crt1 repressor. *Cell* 94: 595 – 605

Ira G, Malkova A, Liberi G, Foiani M, Haber JE (2003) Srs2 and Sgs1-Top3 suppress crossovers during double-strand break repair in yeast. *Cell* 115: 401 – 411

Jansen JG, Tsaalbi-Shtylik A, de Wind N (2015) Roles of mutagenic translesion synthesis in mammalian genome stability, health and disease. *DNA Repair (Amst)* 29: 56 – 64

Kamimura Y, Masumoto H, Sugino A, Araki H (1998) Sld2, which interacts with Dpb11 in *Saccharomyces cerevisiae*, is required for chromosomal DNA replication. *Mol Cell Biol* 18: 6102 – 6109

Klein HL, Symington LS (2012) Sgs1 - The maestro of recombination. *Cell* 149: 257 – 259

Kumar S, Burgers PM (2013) Lagging strand maturation factor Dna2 is a component of the replication checkpoint initiation machinery. *Genes Dev* 27: 313 – 321

Lanz MC, Oberly S, Sanford EJ, Sharma S, Chabes A, Smolka MB (2018) Separable roles for Mec1/ATR in genome maintenance, DNA replication, and checkpoint signaling. *Genes Dev* 32: 822 – 835

Lanz MC, Dibitetto D, Smolka MB (2019) DNA damage kinase signaling: checkpoint and repair at 30 years. *EMBO J* 38: e101801

Lanz MC, Yugandhar K, Gupta S, Sanford EJ, Faça VM, Vega S, Joiner AMN, Fromme JC, Yu H, Smolka MB (2021) In-depth and 3-dimensional exploration of the budding yeast phosphoproteome. *EMBO Rep* 22: e51121

Lazzaro F, Sapountzi V, Granata M, Pellicioli A, Vaze M, Haber JE, Plevani P, Lydall D, Muzi-Falconi M (2008) Histone methyltransferase Dot1 and Rad9 inhibit single-stranded DNA accumulation at DSBs and uncapped telomeres. *EMBO J* 27: 1502 – 1512

Liu Y, Cussiol JR, Dibitetto D, Sims JR, Twayana S, Weiss RS, Freire R, Marini F, Pellicioli A, Smolka MB (2017) TOPBP1Dpb11 plays a conserved role in homologous recombination DNA repair through the coordinated recruitment of 53BP1Rad9. *J Cell Biol* 216: 623 – 639

Lo Y-C, Paffett KS, Amit O, Clikeman JA, Sterk R, Brenneman MA, Nickoloff JA (2006) Sgs1 regulates gene conversion tract lengths and crossovers independently of its helicase activity. *Mol Cell Biol* 26: 4086 – 4094

Longtine MS, McKenzie A, Demarini DJ, Shah NG, Wach A, Brachat A, Philippsen P, Pringle JR (1998) Additional modules for versatile and economical PCR-based gene deletion and modification in *Saccharomyces cerevisiae*. *Yeast* 14: 953 – 961

Majka J, Burgers PMJ (2003) Yeast Rad17/Mec3/Ddc1: a sliding clamp for the DNA damage checkpoint. *Proc Natl Acad Sci USA* 100: 2249 – 2254

Majka J, Binz SK, Wold MS, Burgers PMJ (2006a) Replication protein a directs loading of the DNA damage checkpoint clamp to 5′-DNA junctions. *J Biol Chem* 281: 27855 – 27861

Majka J, Niedziela-Majka A, Burgers PMMJ (2006b) The checkpoint clamp activates Mec1 kinase during initiation of the DNA damage checkpoint. *Mol Cell* 24: 891 – 901

Mankouri HW, Ashton TM, Hickson ID (2011) Holliday junction-containing DNA structures persist in cells lacking Sgs1 or Top3 following exposure to DNA damage. *Proc Natl Acad Sci USA* 108: 4944 – 4949

Mer G, Botuyan MV (2017) A new BRCT binding mode in TopBP1-BLM helicase interaction. *Structure* 25: 1471 – 1472

Mimitou EP, Symington LS (2009) Nucleases and helicases take center stage in homologous recombination. *Trends Biochem Sci* 34: 264 – 272

Mirzaei H, Syed S, Kennedy J, Schmidt KH (2011) Sgs1 truncations induce genome rearrangements but suppress detrimental effects of BLM overexpression in *Saccharomyces cerevisiae*. *J Mol Biol* 405: 877 – 891

Morawska M, Ulrich HD (2013) An expanded tool kit for the auxin-inducible degron system in budding yeast. *Yeast* 30: 341 – 351

Mordes DA, Nam EA, Cortez D (2008) Dpb11 activates the Mec1-Ddc2 complex. *Proc Natl Acad Sci USA* 105: 18730 – 18734

Moynahan ME, Jasin M (2010) Mitotic homologous recombination maintains genomic stability and suppresses tumorigenesis. *Nat Rev Mol Cell Biol* 11: 196 – 207

Myung K, Datta A, Kolodner RD (2001) Suppression of spontaneous chromosomal rearrangements by S phase checkpoint functions in *Saccharomyces cerevisiae*. *Cell* 104: 397 – 408

Navadgi-Patil VM, Burgers PM (2009) The unstructured C-terminal tail of the 9-1-1 clamp subunit Ddc1 activates Mec1/ATR via two distinct mechanisms. *Mol Cell* 36: 743 – 753

Nielsen I, Bentsen IB, Andersen AH, Gasser SM, Bjergbaek L (2013) A Rad53 independent function of Rad9 becomes crucial for genome maintenance in the absence of the RecQ helicase Sgs1. *PLoS One* 8: e81015

Nishimura K, Fukagawa T, Takisawa H, Kakimoto T, Kanemaki M (2009) An auxin-based degron system for the rapid depletion of proteins in nonplant cells. *Nat Methods* 6: 917 – 922

Ohouo PY, Bastos de Oliveira FM, Almeida BS, Smolka MB (2010) DNA damage signaling recruits the Rtt107-Slx4 scaffolds via Dpb11 to Mediate replication stress response. *Mol Cell* 39: 300 – 306

Ohouo PY, Bastos De Oliveira FM, Liu Y, Ma CJ, Smolka MB (2013) DNA-repair scaffolds dampen checkpoint signalling by counteracting the adaptor Rad9. *Nature* 493: 120 – 125

Paciotti V, Clerici M, Lucchini G, Longhese MP (2000) The checkpoint protein Ddc2, functionally related to *S. pombe* Rad26, interacts with Mec1 and is regulated by Mec1-dependent phosphorylation in budding yeast. *Genes Dev* 14: 2046 – 2059

Pfander B, Diffley JFX (2011) Dpb11 coordinates Mec1 kinase activation with cell cycle-regulated Rad9 recruitment. *EMBO J* 30: 4897 – 4907

Piazza A, Shah SS, Wright WD, Gore SK, Koszul R, Heyer WD (2019) Dynamic processing of displacement loops during recombinational DNA repair. *Mol Cell* 73: 1255 – 1266.e4

Puddu F, Granata M, Di Nola L, Balestrini A, Piergiovanni G, Lazzaro F, Giannattasio M, Plevani P, Muzi-Falconi M (2008) Phosphorylation of the budding yeast 9-1-1 complex is required for Dpb11 function in the full activation of the UV-induced DNA damage checkpoint. *Mol Cell Biol* 28: 4782 – 4793

Putnam CD, Kolodner RD (2017) Pathways and mechanisms that prevent genome instability in *Saccharomyces cerevisiae*. *Genetics* 206: 1187 – 1225

Savitsky K, Bar-Shira A, Gilad S, Rotman G, Ziv Y, Vanagaite L, Tagle DA, Smith S, Uziel T, Sfez S *et al* (1995) A single ataxia telangiectasia gene with a product similar to PI-3 kinase. *Science* 268: 1749 – 1753

Schwartz MF, Duong JK, Sun Z, Morrow JS, Pradhan D, Stern DF (2002) Rad9 phosphorylation sites couple Rad53 to the *Saccharomyces cerevisiae* DNA damage checkpoint. *Mol Cell* 9: 1055 – 1065

Seeber A, Dion V, Gasser SM (2013) Checkpoint kinases and the INO80 nucleosome remodeling complex enhance global chromatin mobility in response to DNA damage. *Genes Dev* 27: 1999 – 2008

Segurado M, Diffley JFX (2008) Separate roles for the DNA damage checkpoint protein kinases in stabilizing DNA replication forks. *Genes Dev* 22: 1816 – 1827

Shiloh Y (2003) ATM and related protein kinases: Safeguarding genome integrity. *Nat Rev Cancer* 3: 155 – 168

Shiotani B, Nguyen HD, Håkansson P, Maréchal A, Tse A, Tahara H, Zou L (2013) Two distinct modes of ATR activation orchestrated by Rad17 and Nbs1. *Cell Rep* 3: 1651 – 1662

Stewart JA, Campbell JL, Bambara RA (2009) Dna2 is a structure-specific nuclease, with affinity for 5′-flap intermediates. *Nucleic Acids Res* 38: 920 – 930

Sugawara N, Goldfarb T, Studamire B, Alani E, Haber JE (2004) Heteroduplex rejection during single-strand annealing requires Sgs1 helicase and mismatch repair proteins Msh2 and Msh6 but not Pms1. *Proc Natl Acad Sci USA* 101: 9315 – 9320

Sun L, Huang Y, Edwards RA, Yang S, Blackford AN, Niedzwiedz W, Glover JNM (2017) Structural insight into BLM recognition by TopBP1. *Structure* 25: 1582 – 1588.e3

Tak YS, Tanaka Y, Endo S, Kamimura Y, Araki H (2006) A CDK-catalysed regulatory phosphorylation for formation of the DNA replication complex Sld2-Dpb11. *EMBO J* 25: 1987 – 1996

Tercero JA, Longhese MP, Diffley JFX (2003) A central role for DNA replication forks in checkpoint activation and response. *Mol Cell* 11: 1323 – 1336

Ullal P, Vilella-Mitjana F, Jarmuz A, Aragón L (2011) Rtt107 phosphorylation promotes localisation to DNA double-stranded breaks (DSBs) and recombinational repair between sister chromatids. *PLoS One* 6: e20152

Villa M, Bonetti D, Carraro M, Longhese MP (2018) Rad9/53 BP 1 protects stalled replication forks from degradation in Mec1/ ATR -defective cells. *EMBO Rep* 19: 351 – 367

W.-L. Toh G, Sugawara N, Dong J, Toth R, Lee SE, Haber JE, Rouse J (2010) Mec1/ Tel1-dependent phosphorylation of Slx4 stimulates Rad1-Rad10-dependent cleavage of non-homologous DNA tails. *DNA Repair (Amst)* 9: 718 – 726

Wang J, Chen J, Gong Z (2013) TopBP1 controls BLM protein level to maintain genome stability. *Mol Cell* 52: 667 – 678

Wang J, Chen J, Gong Z (2015) TopBP1 stabilizes BLM protein to suppress sister chromatid exchange. *Mol Cell* 57: 955 – 956

Wanrooij PH, Burgers PM (2015) Yet another job for Dna2: checkpoint activation. *DNA Repair (Amst)* 32: 17 – 23

Wardlaw CP, Carr AM, Oliver AW (2014) TopBP1: A BRCT-scaffold protein functioning in multiple cellular pathways. *DNA Repair (Amst)* 22: 165 – 174

West SC, Blanco MG, Chan YW, Matos J, Sarbajna S, Wyatt HDM (2016) Resolution of recombination intermediates: mechanisms and regulation. *Cold Spring Harb Symp Quant Biol* 80: 103 – 109.

Yu X, Chini CCS, He M, Mer G, Chen J (2003) The BRCT domain is a phospho-protein binding domain. *Science* 302: 639 – 642

Zhang L, Elias JE (2017) Relative protein quantification using tandem mass tag mass spectrometry. *Methods Mol Biol* 1550: 185 – 198

Zhu Z, Chung WH, Shim EY, Lee SE, Ira G (2008) Sgs1 helicase and two nucleases Dna2 and Exo1 resect DNA double-strand break ends. *Cell* 134: 981 – 994

Zou L, Elledge SJ (2003) Sensing DNA damage through ATRIP recognition of RPA-ssDNA complexes. *Science* 300: 1542 – 1548